CHEMICAL ENGINEERING SCIENCE
GENIE CHIMIQUE

VOL. 3 FEBRUARY 1954 NO. 1

Circulation inside gas bubbles

F. H. GARNER and D. HAMMERTON

Department of Chemical Engineering, The University, Birmingham, 15

(*Received* 1 *December* 1953)

Summary—The movement inside rising bubbles has been investigated by visual and indirect means. Gas bubbles of smaller diameter than 0·03 cm in water behave as rigid spheres, and above this diameter a vigorous toroidal circulation sets in, which persists throughout the rise. The transition from rigid to circulating conditions has been determined for several liquids, and it has been found that the critical radius of transition is not in accordance with the formula put forward by BOND and NEWTON.

The velocities of bubbles in water have been measured and the discrepancies between the data in the literature have been considered in terms of four variables: temperature, rate of formation, wall effect and contamination from surface active agents.

Résumé—Les auteurs étudient par l'observation visuelle ou par des méthodes indirectes le mouvement à l'intérieur des bulles gazeuses au cours de leur ascension. Pour des diamètres inférieurs à 0,03 cm., les bulles gazeuses se comportent dans l'eau comme des sphères rigides. Pour des diamètres plus grands, il s'établit une active circulation toroïdale qui persiste tout au cours de l'ascension.

Les auteurs ont déterminé pour différents liquides le seuil de passage de l'état rigide à l'état circulatoire : ils ont trouvé que le diamètre critique de transition ne correspond pas aux valeurs déduites d'une formule proposée par BOND et NEWTON. Ils ont mesuré les vitesses des bulles dans l'eau et les écarts que présentent les différentes valeurs trouvées dans la littérature ont été examinés par rapport aux quatre facteurs : température, vitesse de formation, effet de paroi, contamination de la surface par des agents tensio-actifs.

INTRODUCTION

The velocities of rise of a range of sizes of gas bubbles in water were required for mass transfer calculations, and the internal motion in bubbles was investigated in order to interpret the results. A recent survey [8] of the available data on velocity of rise of bubbles revealed serious disgreements in the diameter range from 0·06 to 0·1 cm.

In fluid droplets or gas bubbles the existence of a regular current of fluid up the central axis and down the sides of the drop had been predicted [15], [29] and demonstrated [11], [12], [13] to be due to the viscous drag of the outer fluid. The velocity of rise with internal circulation as postulated by Hadamard [15] should be 1·5 times that of bubbles in which no circulation occurs – that is of bubbles which behave as though they had the rigid surface of a solid sphere. This ratio of the actual velocity to the theoretical velocity calculated from STOKES' law can be used as an indication [4] of the existence of circulation, and is denoted as $\frac{1}{k}$ in the equation

$$V = \frac{1}{k}(\Delta\rho\, g\, d^2/18\mu) \qquad (1)$$

where V is the velocity of the bubble; $\Delta\rho$ the density difference between phases; g the acceleration due to gravity and μ the absolute viscosity of the outer phase. The value of $\frac{1}{k}$ of 1·5 for a

circulating bubble and 1·0 for a non-circulating bubble holds only in the range of Reynolds' number where Stokes' law is valid. Stokes' law for rigid spheres or for gas bubbles or liquid droplets behaving as rigid spheres is normally only valid for Reynolds' numbers appreciably below 1. If the velocity of circulation in gas bubbles or liquid droplets is as postulated by Hadamard, that is equivalent to the rate of fall or rise of the sphere, then the stream lines will be similar to those in the Stokesian region which therefore should extend considerably higher than 1. Thus we can use $\frac{1}{k}$ at much higher Reynolds' numbers than those in which it is normally assumed that Stokes' law holds. It must also be assumed that there is no distortion of the droplet or bubble shape from a sphere although in fact such distortion does occur at relatively low Reynolds' numbers for air bubbles.

Bond and Newton [4] determined the transition diameter in four systems : air in waterglass, air in *Golden Syrup*, (sugar solution), mercury in *Golden Syrup* and water in castor oil. An attempt was made to characterise the transition region by the dimensionless group RT/W which reduced to a critical radius defined as :

$$r = (T/\Delta\rho\, g)^{\frac{1}{2}} \qquad (2)$$

Observation of Circulation

Motion inside gas bubbles was investigated by the addition of ammonium chloride fog during formation. The most suitable method was to bring together streams of air containing ammonia and hydrogen chloride with one component in excess. Jets of different shapes, both upright and inverted, were used and demonstrated that circulation was not due to the energy of the gas leaving the jet.

The liquids studied were glycerol, white hydrocarbon oil and water. In liquids of viscosity less than 1 poise it was not possible to observe movement in very small bubbles (smaller than 0·35 cm dia.) or in any very rapid bubbles.

Glycerol

Circulation was observed at diameters between 0·44 cm and 1·2 cm. The velocities of bubbles

Table 1. *Divergence from* Stokes' *law of bubbles in glycerol.*

Bubble dia. cm.	Bubble velocity cm/sec	N_{Re}	Wall Effect	$1/k$ (corrected)
Air with Fog				
0·395	1·05	0·041	15%	1·3
0·418	1·1	0·046	15%	1·22
0·443	1·3	0·057	16%	1·26
0·496	1·86	0·093	18%	1·5
0·60	2·43	0·146	23%	1·38
0·67	2·9	0·195	25%	1·35
1·2	5·7	0·68	45%	0·96
Carbon Dioxide				
0·267	0·445	0·010	7%	1·47
0·306	0·534	0·0135	8%	1·34
0·359	0·874	0·026	9%	1·60
0·363	0·878	0·026	9%	1·60
0·478	1·45	0·057	10%	1·53
0·488	1·51	0·061	11%	1·53
0·610	2·24	0·113	14%	1·51
0·640	2·51	0·133	15%	1·58
Air				
0·142	0·103	0·00123	3·0%	1·00
0·162	0·137	0·00180	3·4%	1·03
0·205	0·225	0·00390	4·3%	1·07
0·235	0·371	0·0073	5·0%	1·37
0·249	0·403	0·0083	5·2%	1·33
0·364	0·93	0·027	8·7%	1·33
0·382	1·09	0·048	9·2%	1·42
0·444	1·53	0·067	10·6%	1·50
0·458	1·63	0·082	11·4%	1·50
0·500	1·85	0·093	12·0%	1·46
0·530	2·03	0·113	12·5%	1·44
0·575	2·36	0·136	13·8%	1·42
0·580	2·62	0·165	14·4%	1·55
0·666	3·20	0·232	16·5%	1·48
0·732	3·50	0·280	18·0%	1·35
0·760	3·68	0·313	20·0%	1·34
1·03	6·67	0·72	24·8%	1·37
1·20	7·78	0·98	29·0%	1·22
1·28	8·75	1·12	31·0%	1·22
1·42	9·35	1·39	34·0%	1·09
1·51	9·67	1·53	36·6%	1·02
Sulphur dioxide				
0·283	0·622	0·017	6·8%	1·44
0·299	0·767	0·023	7·2%	1·61
0·399	1·29	0·051	9·5%	1·36
0·416	1·30	0·054	10·0%	1·44
0·624	2·80	0·175	15·0%	1·46

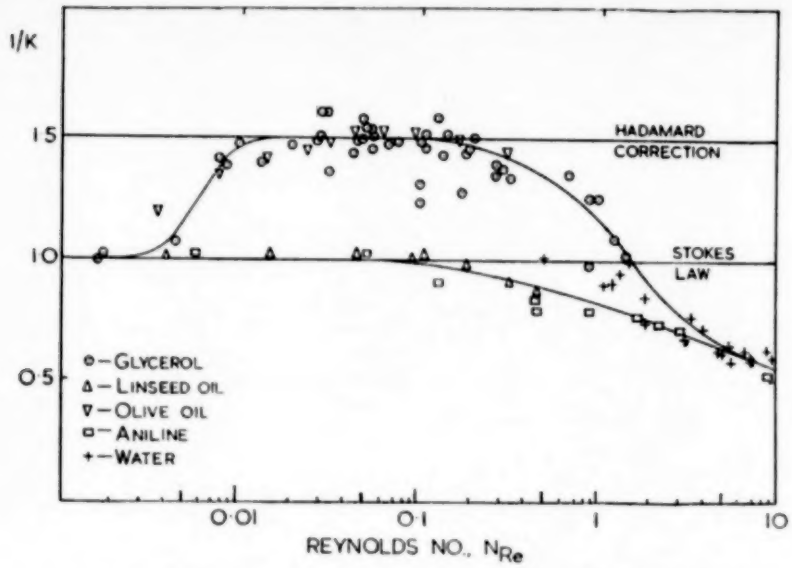

Fig. 1. Divergence of the rate of rise of bubbles from STOKES' law.

with and without fog were measured, and expressed in terms of $\frac{1}{k}$ (Table 1). Fig. 1 shows the results in dimensionless form. At diameters below 0·20 cm ($N_{Re} = 0{\cdot}002$), the value of $\frac{1}{k}$ is 1·0 which indicates that the surface is rigid ; above 0·30 cm ($N_{Re} = 0{\cdot}023$) there is agreement with HADAMARD'S correction, thus confirming the visual observations. The transition diameter between the two regimes was defined by BOND and NEWTON [4] as the value of d when $\frac{1}{k} = 1{\cdot}25$ and for this system it is 0·25 cm $\pm$ 20%.

The full curve in Fig. 1 through the points for glycerol falls sharply from $\frac{1}{k} = 1{\cdot}5$ at $N_{Re} =$ 0·2 and becomes identical with the curve for rigid bubbles, the lower curve, at $N_{Re} = 6{\cdot}0$. Thus the value of $\frac{1}{k}$ cannot be used to detect circulation in bubbles with REYNOLDS' numbers of 6 or over, and, as mentioned later, the bubbles are no longer spherical.

White Oil

Streams of bubbles containing fog were injected into a hydrocarbon oil (viscosity 1·98 stokes at 20°C) at a frequency of 0·1 to 3 per second. Circulation was observed over the diameter range 0·3 to 0·5 cm. ($N_{Re} = 0{\cdot}5 - 1{\cdot}8$). The values of $\frac{1}{k}$ were all greater than 1·5 owing to the rapid rate of formation. Values as high as 2·5 were obtained at frequencies higher than 3 bubbles per sec.

A further series of velocity determinations was made with single bubbles with diameters from 0·04 cm to 0·25 cm. The bubbles were formed without fog, and were measured in a thermometer capillary. The results given in Table 2 agree with HADAMARD'S equation at all diameters. The transition diameter is therefore less than 0·04 cm.

Water

The transition diameter for water could not be observed directly, but could be calculated approximately from values [1] of $\frac{1}{k}$ and from data on mass transfer from bubbles. Below 0·015 cm dia. ($N_{Re} < 1{\cdot}1$) the value of $\frac{1}{k}$ is 1·0 (within 3%) and therefore the bubbles rise as rigid spheres.

Table 2. *Hydrocarbon white oil.*

Bubble dia. cm.	Bubble velocity cm/sec	N_{Re}	Wall Effect	l/k (corrected)
0·036	0·063	0·00124	5%	1·75
0·064	0·137	0·00475	10%	1·25
0·066	0·195	0·00695	10%	1·62
0·085	0·268	0·0122	13%	1·44
0·116	0·476	0·0297	19%	1·44
0·117	0·515	0·0327	20%	1·52
0·125	0·592	0·040	21%	1·55
0·254	2·08	0·285	43%	1·57
0·254	1·88	0·257	43%	1·42

The rate of mass transfer from bubbles of 0·03 cm dia. is reported [26] to be 45 cm/hr, and for a circulating bubble is 170 cm/hr. Circulation therefore starts between 0·015 and 0·03 cm dia., but it does not reach the maximum speed until 0·25 cm dia. [16].

Circulation in bubbles can be observed if the viscosity of water is increased to 115 c.p. by addition of 2% of *Cellofas B*, a hydroxylated cellulose. Circulation was observed with bubbles larger than 0·3 cm dia., and the transition diameter was between 0·3 and 0·5 cm as shown both by mass transfer data and by values of $\frac{1}{k}$. A similar value for transition diameter was observed for a 1% solution having a viscosity of 30 c.p.

It is shown later that circulation at all diameters up to at least 0·6 cm can be stopped by very small quantities of surface active materials adsorbed on the bubble. It is inferred that the "condensed solid" type of film [17] is formed, making the surface rigid.

Data from the literature

ARNOLD [2] reported the velocity of bubbles in olive oil and linseed oil, from which values of $\frac{1}{k}$ were calculated. His results show that in olive oil, circulation starts at 0·01 cm dia. and is fully established at 0·07 cm dia. Above this diameter there is agreement with the Hadamard equation (Fig. 1). Bubbles in linseed oil have a value of 1·0 (within 3%) until inertia effects become important at $N_{Re} = 0{\cdot}2$.

Table 3. *Transition radius, cm.*

System	Observed radius	Bond theoretical radius	Reference
Air in waterglass	0·11	0·25	BOND and NEWTON [4]
Air in syrup	0·11	0·25	
Mercury in syrup	0·12	0·30	
Water in castor oil	0·77	0·70	
Air in white oil	< 0·06	0·12	
Air in glycerol	0·125	0·225	Present Work
Air in water	0·020	0·27	
Air in water + 2% *Cellofas*	0·25	0·25	
Air in aniline	> 0·05	0·42	ALLEN [1]
Air in olive oil	0·04	0·173	ARNOLD [2]
Air in linseed oil	> 0·15	—	ARNOLD [2]

DISCUSSION

In Table 3 are given the observed transition radius and that calculated by BOND and NEWTON's equation (2). There is a marked divergence, between these values and only for water in castor oil and for air in a *Cellofas* solution is there good agreement.

The failure of equation (2) to predict the transition diameter implies that other variables exert an influence on circulation, and the movement of the surface must be considered in more detail. The surface of the bubble moves outwards and downwards from the forward stagnation point, thus forming new surface. The energy required per second to form the surface is $2\pi r Tu$ ergs, where u is the tangential velocity of the surface at the "equator" of the sphere and T is the interfacial tension, dynes/cm. This energy is given up from the rear of the bubble by the closing up of the surface, and there may be a net loss of energy if the interfacial tension in compression is less than in stretching. BRYN [5] refers to this difference as the relaxation effect.

VOL. 3 1954

Table 4.

Diameter cm	Velocity cm/sec.	Temperature °C	N_{Re}
Air bubbles in 10 cm dia. column			
0·0186	1·45	14·6	2·3
0·0258	1·96	14·6	4·4
0·0307	2·70	14·6	7·2
0·0313	2·82	14·0	7·7
0·0321	2·82	13·5	7·7
0·0326	3·17	14·3	8·9
0·0357	3·50	14·6	11·2
0·0357	3·45	14·0	10·5
0·0402	4·02	14·6	14·1
0·0417	3·72	14·3	13·4
0·0428	4·34	14·6	16·5
0·0490	5·43	14·0	22·8
0·0512	5·75	14·0	25·1
0·0522	5·65	12·5	24·3
Air bubbles in 2 cm dia. column			
0·0126	0·707	15·0	0·9
0·0135	0·85	15·0	1·0
0·0203	1·48	15·0	3·0
0·0252	2·26	15·0	5·6
0·0336	2·65	15·0	8·9
0·0359	3·22	15·0	11·5
0·0572	5·4	15·0	31·0
Air bubbles in 10 cm dia. column			
0·307	24·6	18·0	720
0·314	24·6	18·0	740
0·400	24·0	18·0	910
0·425	23·4	16·0	940
0·441	22·2	18·0	930
0·460	21·6	18·0	950
0·483	23·2	16·0	1070
0·492	23·2	16·0	1090
0·499	22·7	18·0	1080
0·504	22·0	18·0	1060
0·675	23·0	16·0	1550
Ethylene bubbles in 10 cm dia. column			
0·1	10·8	17·0	103
0·16	15·0	17·0	212
0·2	21·7	17·0	420
0·23	22·4	17·0	490
0·25	22·6	17·0	530
0·26	23·3	17·0	570
0·28	23·2	17·0	610
0·29	24·6	17·0	670
0·32	22·7	17·0	690
0·344	23·8	17·0	760
0·453	22·6	17·0	950

Table 5. Rate of rise of bubbles contaminated with 'Vaseline.'

Diameter cm	Velocity cm/sec	Temperature °C	Time since previous bubble
Air bubbles			
0·216	18·3	14·0	30 min.
0·222	18·4	14·5	90 min.
0·281	18·9	16·0	10 min.
0·282	18·9	14·0	12 hr.
0·291	20·3	16·0	72 hr.
0·339	19·5	18·7	—
0·365	20·1	16·0	20 min.
0·373	20·2	16·0	60 min.
0·423	20·6	18·7	5 min.
0·440	21·0	16·0	20 min.
0·444	21·1	14·5	12 hr.
0·454	20·5	14·5	20 min.
0·455	21·1	14·5	30 min.
0·484	21·4	14·5	—
0·525	21·5	14·7	—
0·518	20·3	17·0	12 hr.
0·534	21·1	15·0	—
0·550	21·0	20·0	30 min.
0·573	21·0	20·0	2 hr.
0·575	21·8	15·2	—
0·619	22·[illegible]	17·0	—
0·655	22·5	17·0	—
0·678	22·6	14·7	2 hr.
0·745	23·3	17·2	—
0·783	23·1	15·0	90 min.
Ethylene bubbles			
0·253	18·7	17·0	—
0·374	20·4	17·0	—
0·435	20·9	17·0	—
0·528	21·0	17·0	—
0·634	22·2	17·0	—
0·737	22·8	17·0	—

Thus any change of surface tension with time would be an important factor in determining the start of circulation, since if the work done on the bubble by the skin friction is less than any nett loss of surface energy, the circulation cannot persist.

The transition diameter can only be completely correlated for all systems if terms for the intensity of skin friction and for the change of interfacial tension with time are included in the expression. More data are required on transition diameters

for pure systems and for those containing surface active agents.

Measurement of Velocity

The velocity of small bubbles was measured with a stop watch over a rise of 73 cm. Columns of 10 cm and 2 cm dia. were used, containing water saturated with air. Bubbles of diameters down to 0·0125 cm were formed singly in a thermometer capillary [7] of 0·005 cm dia. Below 0·010 cm dia. the errors of measurement are greater than 10% by this method owing to the curvature of the meniscus of the confining liquid.

Oscillation and Change of Shape

Bubbles smaller than 0·1 cm diameter are approximately spherical and rise in straight vertical lines. At a critical diameter reported by Hoefer [18] as 0·10 cm and by Bryn [5] and Luchsinger [20] as 0·15 cm, the path of rise becomes a helix. The pitch and the amplitude of the helix are both approximately two diameters. The bubble is flattened into a lenticular shape, and moves in the direction of the major axes.

The dimensions of the helix increase with the diameter up to 0·5 cm diameter, when periods of straight vertical rise interrupt the helix. Bubbles bigger than 0·8 cm diam. nearly always

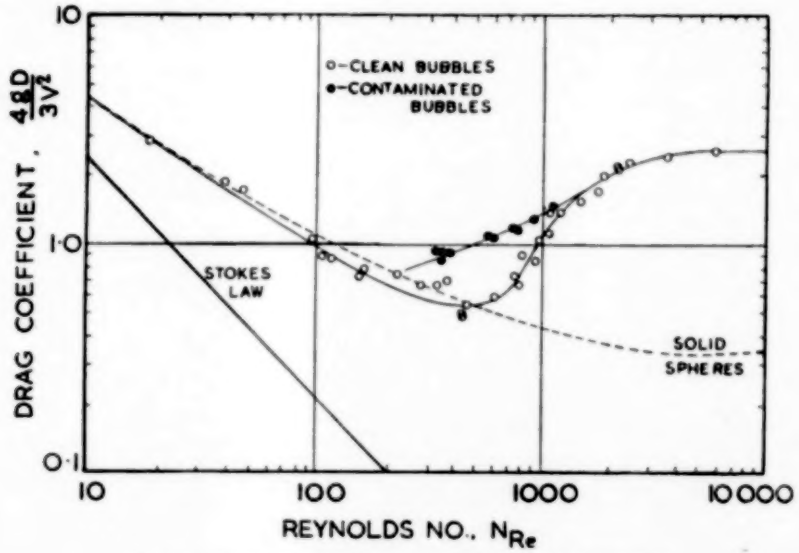

Fig. 2. Correlation of drag coefficient and Reynolds' No. for bubbles in water.

Larger bubbles of 0·15 cm to 0·8 cm diameter rise too rapidly for accurate timing by stop watch. A cinephotographic method was used, having a repeatability of 1%. The cine camera was brought to focus through a system of mirrors on two marks 56 cm apart on the column. The camera speed was found to be constant within 1% over both long and short periods, at a speed of 18·4 frames/sec. Scrupulous care was necessary in the cleanliness of the apparatus to obtain consistent results.

rise in straight lines. Their shape is hemispherical in front and flattened at the rear. Changes of shape are confined to irregular swinging of the rear part. Bryn and Hoefer report similar observations, but Coppock and Meiklejohn [7] recorded that when bubbles rise in series the times of rise are erratic.

Some bubbles in our work did not rise in the usual helical manner, but followed a zig-zag path, moving bodily from side to side in one vertical plane. This type of oscillation was found

VOL. 3 1954

to be due to contamination from *Vaseline* used as a lubricant on the plug of a wide-bore glass tap. The bubble was held below the tap before being released into the timing section of the column. During this residence time, surface active constituents of the *Vaseline* were adsorbed onto the surface of the bubble, and mass transfer data [16] later showed that the surface was being prevented from circulating by a hydrocarbon film.

EXPERIMENTAL RESULTS

Table 4 gives the measured velocities of single bubbles in water, and Fig. 2 compares them in dimensionless form with the drag curve for solid spheres [6]. Bubbles smaller than 0·1 cm dia. ($N_{Re} = 100$) have about the same drag coefficient as solid spheres. At higher REYNOLDS' numbers, the drag is less than for a solid sphere, even though the distance to be travelled along the helical path is greater than the vertical distance. This is because the bubble is flattened, and presents a considerably smaller frontal area [22] in the direction of motion than a sphere of equal volume.

The velocities of bubbles whose surfaces are contaminated with surface active molecules (Table 5) do not show these low drag coefficients at $N_{Re} = 200$ to $N_{Re} = 1{,}200$. Fig. 2 shows that the drag is greater than on either solid spheres or clean bubbles. At very high REYNOLDS numbers the drag coefficient becomes constant [9] at a value of 2·8. This value is higher than for a spherical body of the same volume because a greater frontal area is presented in the direction of motion. This difference in the direction of clean and contaminated bubbles has been referred to previously.

The graphical presentation of data as a logarithmic plot is not altogether satisfactory, since the accuracy of values taken from the curve is poor. A linear plot of velocity against diameter has been preferred in this work. Fig. 3 shows the experimental data for clean bubbles, and Fig. 4 the effect of contaminants on the rate of rise.

The smallest bubbles are in agreement with the results of ALLEN [1] and COPPOCK [7]. The

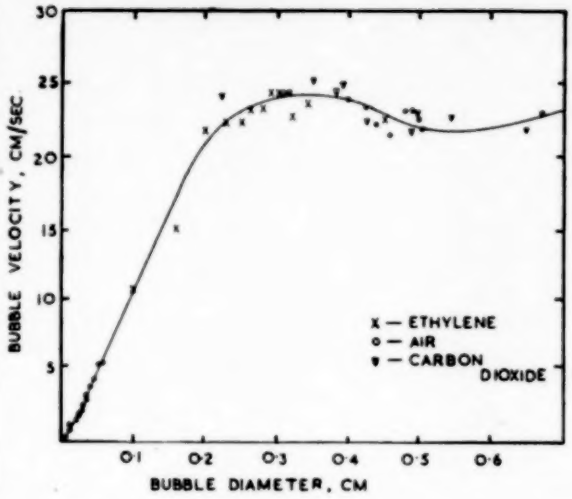

Fig. 3. Velocity of gas bubbles in water.

velocities are represented by the equations

$$V = 103d \text{ for } 0{\cdot}01 < d < 0{\cdot}04 \text{ cm} \quad (3)$$

$$V = 108\,d \text{ for } 0{\cdot}04 < d < 0{\cdot}20 \text{ cm} \quad (4)$$

In the diameter range 0·2 cm to 0·6 cm figures in the literature vary widely, since it is in this region that the four major variables

(a) time interval between bubbles
(b) surface contamination
(c) temperature
(d) wall effect

have caused wide discrepancies. The effects of these variables are discussed below.

TIME INTERVAL BETWEEN BUBBLES

The interaction between successive bubbles rising in the same vertical path has been calculated [3] for the STOKES' law region. At high REYNOLDS' numbers, the data available (Fig. 5) show that when bubbles are separated by less than 3 seconds the velocity is appreciably higher than for the single bubbles shown in the lower curve. The difference was found to be as much as threefold [8] at frequencies above 1 per second.

MIYAGI quotes results that differ markedly from the present data, and although he states that formation was " very slow," it is evident

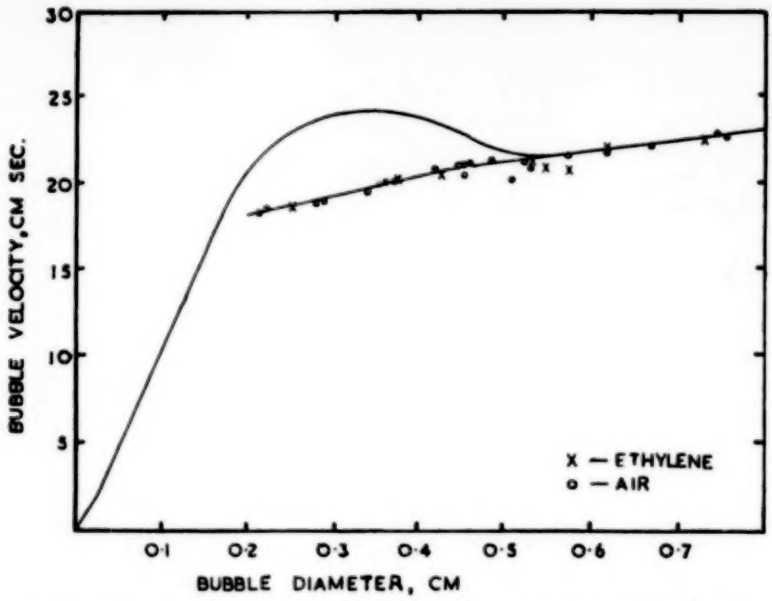

Fig. 4. Velocity of single bubbles with surfaces contaminated by *Vaseline*.

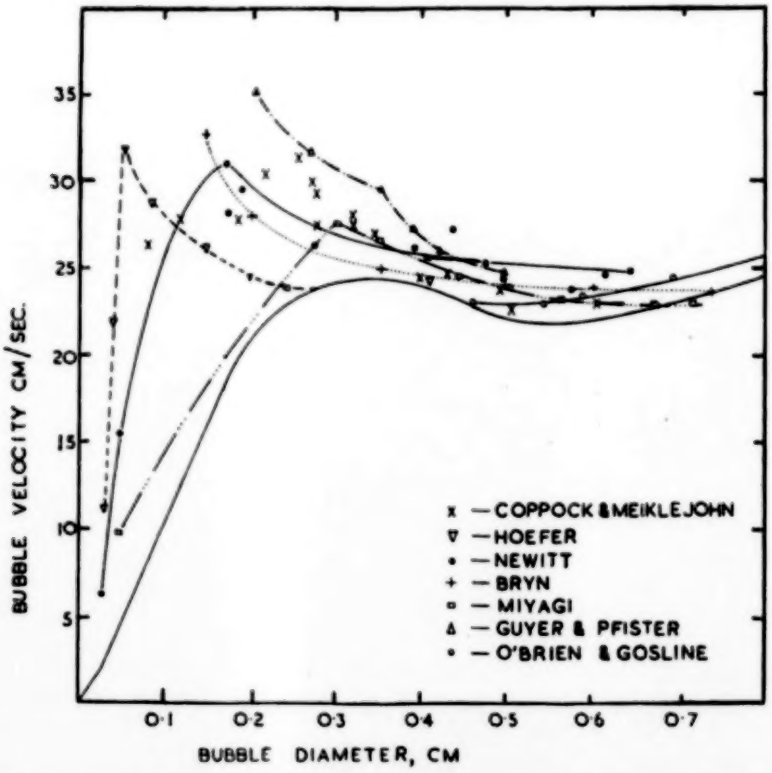

Fig. 5. Velocity of streams of bubbles rising in water, compared with that of single bubbles.

VOL. 3 1954

from his description of the photographic recording that bubbles were in fact formed at approximately 1 per second.

Coppock and Meiklejohn [7] formed bubbles at one per second, and the velocities were found to be from 2% to 30% greater than those of single bubbles. Accurate detailed study showed that the velocity over 10 cm. intervals varied by as much as 20% from the terminal velocity over 200 cm. The variation was random, and was not observed with single bubbles. The frequency was about 1 per sec. Other workers [8], [19] [23], [24] have demonstrated the higher velocity of streams of bubbles at diameters above 0·5 cm.

It can be concluded that the error due to interaction of successive bubbles is less than 1% only when the interval between them is greater than 3 seconds.

Surface Contamination

The cause of the lower velocity of contaminated

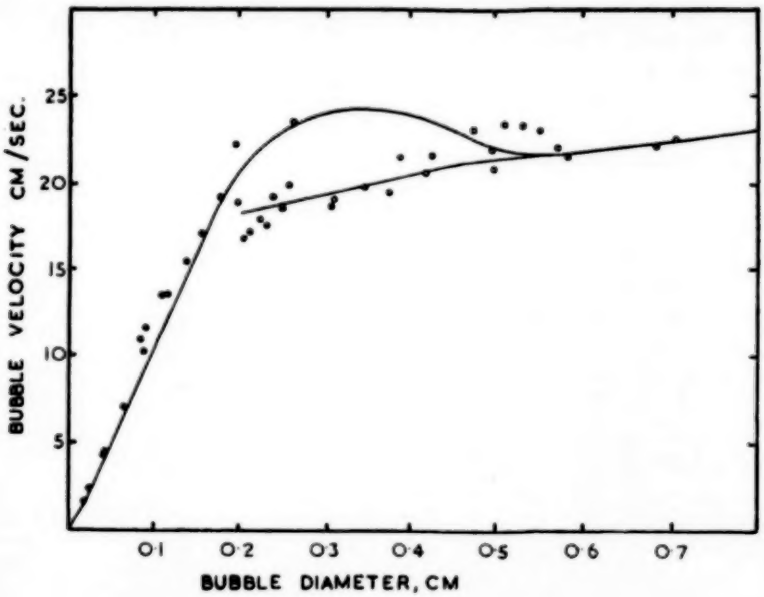

Fig. 6. Comparison of the data of Coppock and Meiklejohn with the curve for contaminated bubbles (from Fig. 4). Circles are data of Coppock and Meiklejohn and the curve and line are taken from Fig. 4.

irregularity of motion in streams of bubbles may account for many of the discordant results in the literature.

Guyer and Pfister [14] formed bubbles of carbon dioxide in water in a 3 cm. dia. column at a frequency of 3 per sec. The velocity is from 50% to 12% greater than that of single bubbles.

Bryn [5] and Luchsinger [20] do not report the precise rates of formation. In both cases, bubbles were formed at a glass jet from a continuous supply of gas, and it must be assumed that bubbles as shown in Figure 4 lies mainly in the shape of the oscillation and the greatest difference in velocity lies in the region where oscillation is most pronounced. The length of a helical path is greater than that for a zig zag rise of the same total height. The actual point velocities of contaminated and clean bubbles must therefore be even more widely different than the overall velocities. This appears to be due to the fact that in helical rise the bubble never comes to rest, whereas in a zig zag it " stalls " twice in

every oscillation. Skin friction is negligible compared with form drag at Reynolds' numbers over 100, but cessation of circulation has an effect not only on skin friction but will also cause some increase in form drag.

The data of Coppock and Meiklejohn for single bubbles formed slowly at a jet are compared with the present data in Fig. 6. It appears that some contamination was occurring in their work during the residence on the jet, and possibly lubricant from the controlling needle valve travelled along the metal surfaces to the jet. The scatter of the experimental data is far greater than the error of the method, and may be the result of different degrees of contamination due to different times of contact with the jet.

Temperature

The present experiments covered the range of temperatures from 14°C to 20°C, and no variation of velocity was observed for either clean or contaminated bubbles from 0·2 cm to 0·8 cm. dia.

Data presented by Peebles and Garber [27], however, shows velocities at 0·21 cm and 0·32 cm. dia. to be 40% and 14% higher, respectively, than the present results. The temperature is not reported, but from the values of viscosity and surface tension used it appears to be 33°C. The differences cannot be ascribed to error, since a stop-watch can be read to within 10% in a measurement of 2 sec. The frequency of formation was reported to be 0·1 to 0·06 bubbles per sec., and if this applies to the two smallest bubbles then the difference must be due to viscosity. At diameters above 0·4 cm the velocity does not vary with small changes in temperature and viscosity, and by applying the appropriate wall correction, the data of Peebles and Garber are in agreement with the majority of workers [5], [7], [9], [22], [23].

Wall Effect

The motion of spheres in the region where Stokes' law applies is reviewed extensively by Barr [3]. Corrections for the presence of confining walls have been derived by Ladenberg and by Faxen [3]. The Ladenberg correction is given in equation (5).

Table 6.

Effect of confining walls on the velocity of spheres and bubbles.

d	d/D	K	N_{Re}	System and Author
0·26	0·11	3·4	0·20	Steel spheres in glycerol
0·38	0·17	2·95	0·34	
0·5	0·22	3·3	0·62	
1·0	0·44	1·8	1·75	Lunnon [21]
1·5	0·66	1·37	1·1	
0·02	0·01	0	3·0	Bubbles in water
0·03	0·015	3·5	7·0	
0·04	0·02	5·5	14	
0·05	0·025	6	25	
0·06	0·03	6	38	
0·07	0·035	6	60	
0·08	0·04	7	82	
0·09	0·045	8	105	
0·10	0·05	9	120	Present work
0·3	0·087	1·15	500	Air in water Coppock and Meiklejohn [7]
0·706	0·27	0·66	1810	Air in water
0·835	0·32	0·70	2110	
1·08	0·415	0·71	2720	
1·15	0·44	0·74	2920	Peebles and Garber [27]
1·1	0·141	1·07	3000	Air in water Luchsinger [20]
1·0	0·33	0·69	2000	Air in water
2·0	0·66	0·68	3400	
2·0	0·33	0·64	5000	O'Brien and
2·8	0·18	0·17	9000	Gosline [23]
2·0	0·4	0·35	6000	Air in water Oyama and Iwase [25]
0·64	0·123	0·135	7600	Steel spheres in water
0·96	0·185	0·225	13200	
1·28	0·246	0·25	25600	
1·60	0·308	0·312	25600	
1·98	0·368	0·358	31400	
0·64	0·217	0·154	7400	
0·96	0·326	0·34	12300	
1·28	0·434	0·42	17000	
1·60	0·542	0·40	21000	Lunnon [21]
1·98	0·651	0·49	24800	

VOL. 3 1954

$$V = v\,(1 + 2{\cdot}1\,d/D) \qquad (5)$$

where

V is the velocity in an infinite fluid
v is the velocity in a cylindrical container
D is the diameter of the container
d is the bubble diameter.

The equation applies for values of d/D below 0·1 and for values of N_{Re} below 0·2. At high REYNOLDS' numbers there is no satisfactory correlation. The data of several workers are summarised in Table 6 where the LADENBERG equation has been used as a basis of comparison because of its simplicity. The coefficient of the term d/D is designated K.

The conclusions from Table 6 are that as N_{Re} increases, K decreases : but that for any given column diameter K increases with N_{Re}. The error introduced into determinations of velocity by the wall effect is less than 1% if the column is more than 100 times the diameter of the bubble.

CONCLUSIONS

1. The velocity of a single bubble in water has been determined with an accuracy of 2%.
2. The four major sources of divergence from the true velocity and the limits of their effectiveness have been investigated.
3. The existence of regular circulatory currents in gas bubbles rising through three liquids has been demonstrated.
4. The diameter at which circulation commences in different liquids has been listed, and the Bond criterion has been shown to be unreliable for many of these systems.

NOMENCLATURE

d = diameter of bubble, cm
g = gravitational constant, cm/sec^2.
K = constant in the Ladenberg equation (5)
N_{Re} = REYNOLDS' number,
r = radius of bubble or drop, cm.
T = interfacial surface tension, dynes/cm.
u = tangential velocity of bubble surface, cm/sec.
v = velocity of rise of bubble, cm/sec.
$\frac{1}{k}$ = bubble velocity divided by STOKES' law velocity
Δ_ρ = density difference between phases, g/cc.
μ = viscosity of continuous phase, g/cm. sec.

REFERENCES

[1] ALLEN, H. S. ; Phil. Mag. 1900 Ser. 5, **50** 323 519.
[2] ARNOLD, H. D. ; Phil. Mag. 1911 Ser. 6, **22** 755.
[3] BARR, G. ; A Monograph of Viscometry. O.U.P., 1931.
[4] BOND, N. W. and NEWTON, D. A. ; Phil. Mag. 1928 Ser. 7 **5** 794.
[5] BRYN, T. ; Forsch-Gebiete Ingenieurw, 1933 **4** 27.
[6] Castleman, R. A. ; N.A.C.A. Tech. Note No. 231, Washington, 1926.
[7] COPPOCK, P. D. and MEIKLEJOHN, G. T. ; Trans. Inst. Chem. Engrs. (London). 1951 **29** 75.
[8] DATTA, R. L., NAPIER, D. G. and NEWITT, D. M. ; Trans. Inst. Chem. Engrs. 1950 **28** 14.
[9] DAVIES, R. M. and TAYLOR, G. ; Proc. Roy. Soc. A 1950 **200** 375.
[10] FUCHS, N. ; Trans. Faraday Soc. 1936 **32** 1190.
[11] GARNER, F. H. ; Trans. Inst. Chem. Engrs. 1950 **28** 88.
[12] GARNER, F. H., and HALE, A. R. ; Chem. Eng. Sci. 1953 **2** 157.
[13] GARNER, F. H. and SKELLAND, A. H. P. ; Trans. Inst. Chem. Engrs. 1951 **29** 14.
[14] GUYER, A. and PFISTER, X. ; Helv. chim. acta., 1946 **29** 1173.
[15] HADAMARD, J. ; Compt. Rend. 1911 **152** 1735.
[16] HAMMERTON, D. ; Ph.D. thesis, University of Birmingham 1953.
[17] HARKINS, W. D. ; The Physical Chemistry of Surface Films, 1952.
[18] HOEFER, K. ; Forschungsarbeiten, V.D.I., 1913 **138** 1.
Z. Ver. Deut. Ing. 1913 **57** 1174.
[19] VAN KREVELEN, D. W. and HOFTIZER, P. J., Chem. Eng. Prog. 1950 **46** 29.
[20] LUCHSINGER, W. ; Koll. Z., 1937 **81** 180.
[21] LUNNON, R. G. ; Proc. Roy. Soc., A 1928 **118** 680.
[22] MIYAGI, O. ; Phil. Mag. 1925, Ser. 6, **50** 112.
[23] O'BRIEN, M. P. and GOSLINE, J. E. ; Ind. Eng. Chem. 1935 **27** 1436.
[24] OWENS, J. S. ; Engineering 1921 **112** 159 and 458.
[25] OYAMA, Y. and IWASE, K., Sci. papers Inst. Phys. Chem. Res. Tokyo, 1939 **36** 371.
[26] PATTLE, R. E., Trans. Inst. Chem. Engrs. (London) 1950 **28** 27.
[27] PEEBLES, F. N. and GARBER, H. J. ; Chem. Eng. Prog. 1953 **49** 88.
[28] REMY, H. ; Trans. Faraday Soc. 1936 **32** 1185.
[29] RYBCZNSKI, Bull. Acad, Sci. Cracovie, 1911 **1** 40.

Chemical Engineering Science, 1954, Vol. 3, pp. 12 to 16. Pergamon Press Ltd.

Etude de quelques aspects de la fluidisation dans les liquides

RENÉ JOTTRAND

Service de Chimie Industrielle de l' Université Libre de Bruxelles. 50 avenue F. D. Roosevelt Brussells.

Communication faite au Congrès de Chimie Industrielle de Paris (juin 1953)

(*Received* 28 *November* 1953)

Summary—Experiments and a study of the literature confirm the general equation $u = V\epsilon^{\sigma}$ where u is liquid velocity above the bed, V the free falling velocity of the particles in water and ϵ the fraction of the volume of the bed occupied by liquid, σ depends on the shape of the particles and the turbulence of the fluid. It varies with the free space of the bed at rest ϵ_i.

The law is used to calculate the distance between particles as a fraction of their diameter and the fluid velocity. It is then possible to explain why there is no classification in a concentrated bed.

Experiments with different coloured particles show that classification is due to varying density and not due to variation in the free falling velocity.

Résumé—De nouvelles expériences et une étude bibliographique approfondie confirment qu'il y a intérêt à mettre la relation entre la vitesse et la concentration du lit sous la forme $u = V\epsilon^{\sigma}$. L'exposant σ dépend à la fois de la forme des grains et de la turbulence de l'écoulement. Il varie parallèlement à ϵ_i, fraction de vide dans le lit au repos.

En se basant sur la loi $u/V = \epsilon^{\sigma}$ on calcule les variations des distances entre grains en fonction du diamètre des grains et de la vitesse du fluide. On peut alors expliquer pourquoi il n'y a pas de classement par différence de granulométrie dans un lit concentré.

Des essais de fluidisation avec des solides de couleurs différentes montrent d'autre part que le classement se fait d'après les densités moyennes des suspensions et non d'après les vitesses de chute libre des grains.

Le développement de la catalyse fluide a attiré l'attention des chercheurs sur le mécanisme de la mise en suspension d'une poudre par un courant de fluide ascendant, et sur les propriétés de ces suspensions ; la présente note se limitera à l'étude de quelques aspects importants de la fluidisation dans les liquides.

Le premier problème que nous voulons aborder est celui de la loi d'expansion du lit en fonction de la vitesse du liquide. Ce problème fondamental est, de loin, celui qui a été le plus étudié. Cependant aucune solution définitive n'est encore acquise.

Pour définir l'expansion, nous employons la variable ϵ qui représente la fraction du volume total du lit qui est occupé par le liquide.

Nous avons proposé précédemment [3] la relation.

$$u = V\epsilon^{\sigma}$$

où u est la vitesse ascendante moyenne du liquide, V la vitesse de chute isolée d'un grain moyen et σ un nombre caractéristique des propriétés de la poudre.

Nous pouvons ajouter à présent que cette relation est bien vérifiée par *tous* les résultats expérimentaux qui ont été publiés à notre connaissance [1 à 11]. Elle a le grand avantage d'être simple et d'avoir une représentation linéaire dans un diagramme logarithmique. Elle permet la comparaison facile du comportement des différentes poudres et la mise en évidence d'anomalies dans le comportement de certaines de celles-ci. Elle permet également de préciser l'effet des différentes caractéristiques de la poudre.

En effet, en plus des variables qui interviennent dans le calcul de V, c'est-à-dire le diamètre des grains et leur densité ainsi que la densité et la viscosité du liquide, il faut encore tenir compte de plusieurs facteurs qui ont une influence sur σ :

Ces facteurs qui sont en ordre principal la

forme et la dimension des grains sont difficiles à mesurer avec précision, et nous devons nous contenter d'indications qualitatives.

Nous dirons que l'exposant σ varie, en général, de 2 à 7 pour atteindre dans certains cas la valeur de 10.

Les petites valeurs de σ correspondent à des grains gros et de forme arrondie ou sphérique, les grandes valeurs à une granulométrie fine et à des formes anguleuses et irrégulières.

Il est intéressant de rapprocher les valeurs de σ des propriétés de la poudre en tas que l'on peut caractériser en première approximation par la valeur ϵ_i de la fraction du volume laissé entre les grains au repos.

On constate que les grains gros et sphériques se tassent plus fort que les grains fins et anguleux ; à de faibles valeurs de σ correspondent donc de faibles valeurs de ϵ_i, toutefois une relation quantitative est difficile à établir, car des facteurs tels que la forme des grains ou le tassement d'une poudre sont délicats à mesurer.

Nous nous sommes aussi attachés à une autre question dans laquelle on commet souvent, pensons nous, de graves erreurs. C'est le problème du *classement* qui se produit dans un lit fluidisé ou dans une suspension en train de décanter.

On sait depuis longtemps que pour obtenir un bon classement de substances pulvérulentes par différence des vitesses de sédimentation il est nécessaire de travailler à faible concentration (1% par exemple).

On a remarqué que le classement ne se faisait pas bien avec des suspensions plus concentrées.

D'autre part, dès les premières études de fluidisation, on a été frappé par la netteté du niveau supérieur de lits à granulométrie très étendue ; on a remarqué que cette netteté était plus grande aux fortes concentrations et on a attribué le phénomène aux nombreux chocs entre grains de différentes grosseurs qui auraient pour résultat d'égaliser leurs vitesses.

On a toujours admis que le classement se faisait ou tendait à se faire selon les vitesses de chute libre, c'est-à-dire que les grains à grande vitesse de chute se plaçaient dans le bas, et ceux à faible vitesse dans le haut.

Nous pensons qu'en se basant sur la forme simple de la loi qui unit vitesse et concentration : $u = V \epsilon^{\sigma}$ (1) on peut donner un schéma des phénomènes qui indique pourquoi la classification ne se fait pas dans un lit concentré.

Pour arriver à ce résultat nous faisons quelques hypothèses simplificatrices qui nous permettront de calculer la distance entre les grains en fonction de la vitesse du liquide et de la grosseur des grains.

(1) Nous supposons que nous sommes dans le domaine de STOKES, c'est-à-dire que la vitesse de chute des grains isolés V est proportionnelle au carré du diamètre des grains : $V = k\, d^2$ (2).

(2) On considère des grains sphériques répartis régulièrement dans l'espace, aux noeuds d'un réseau régulier.

(3) On considère encore que l'expansion se fait par augmentation simultanée des distances entre grains sans que les positions relatives soient modifiées.

On en déduit que la fraction du volume occupé par le solide $(1 - \epsilon) = K \left(\frac{d}{D}\right)^3$ (3) où D est la distance entre les centres de grains voisins, et d le diamètre des grains ; K dépend du mode d'empilement et vaut $(1 - \epsilon_i)$, c'est-à-dire la fraction du volume occupé par le solide au repos, quand les grains voisins se touchent $(d = D)$.

En combinant les relations (1), (2), (3) on trouve :

$$u = k\, d^2 \left[1 - (1 - \epsilon_i)\left(\frac{d}{D}\right)^3\right]^{\sigma}$$

relation entre u, d et D que nous avons représentée à la Fig. 1 dans le cas particulier $\sigma = 4$ $\epsilon_i = 0{\cdot}4$, et pour quelques valeurs particulières de u.

Ces courbes présentent un minimum qui permet de séparer deux zones ; dans la partie de droite où le rapport d/D est grand le lit est concentré et les courbes sont ascendantes, alors que dans la partie de gauche où d/D est faible elles sont descendantes.

Considérons d'abord la partie de droite, pour une vitesse $u_A = 0{\cdot}1$ des particules de 75μ sont en équilibre à une distance de 95μ.

Imaginons parmi les autres, une particule plus petite B, pour qu' elle reste à la même

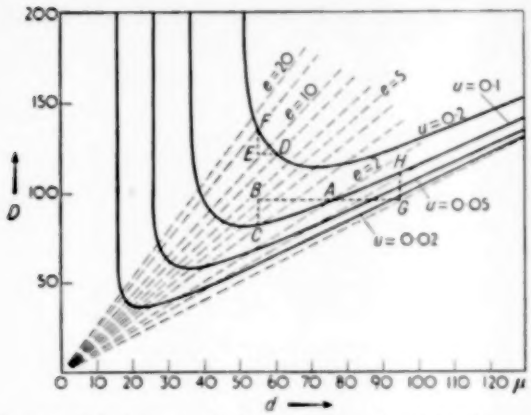

Fig. 1. Relation entre le diamètre de grains *d*, la distance entre les grains *D*, et la vitesse moyenne du liquide *u*.

distance de 95μ de ses voisines il faudrait une vitesse u_B plus grande que u_A.

Cela veut dire que si la vitesse du liquide est u_A cette particule va descendre avec une vitesse $u_B - u_A$, ce faisant elle se raproche de ses voisines inférieures, D diminue et on atteint un nouvel équilibre représenté par le point C.

On voit donc qu'une particule plus petite au lieu d'être entraînée par le courant et de monter comme cela se passe aux faibles concentrations tend dans ce domaine à se rapprocher de la couche inférieure ; inversement une particule plus grosse G trouve sa position d'équilibre en H à une distance plus grande après avoir monté puisque u_A est plus grand que u_G.

On peut illustrer cette explication mathématique et qui n'est évidemment que schématique par l'image suivante.

Considérons quelques grains voisins, supposons que le grain central devienne brusquement plus petit, il y a dans son voisinage une augmentation de la section libre qui provoque une diminution de la vitesse locale réelle du fluide et donc une diminution de la force d'entraînement. Il se peut que cette diminution soit plus que suffisante pour compenser la diminution du poids apparent de la particule ; dans ce cas la particule descendra et viendra trouver une nouvelle position d'équilibre plus proche de ses voisines inférieures.

Dans la partie gauche de la figure, aux faibles concentrations, les courbes sont descendantes, les phénomènes sont inverses, les grains les plus gros ont tendance à descendre, les grains les plus fins à monter ; Ceux-ci peuvent même être entraînés en dehors du lit, qui se dissociera alors en plusieurs zones.

Les points minimum des courbes correspondent aux valeurs limites de l'expansion au-delà desquelles il n'est plus possible d'avoir d'une façon stable un lit homogène avec une limite supérieure bien nette.

On peut montrer qu'on a

$$\epsilon_{max} = (1 - \epsilon_i)\,\frac{2 + 3\sigma}{2} \text{ pour } \sigma = 4\,\epsilon_i = 0{\cdot}4$$

on trouve $\epsilon_{max} = 4{\cdot}2$ ce qui est en bon accord avec l'expérience.

Le mécanisme exposé ci-dessus n'est valable que pour décrire le classement de grains tous de même densité.

L'étude expérimentale que nous avons entreprise pour en vérifier les résultats nous a cependant permis de tirer quelques conclusions concernant le cas de deux matières différentes, ayant des densités différentes.

Nous avons fluidisé dans l'eau des mélanges de poudres de couleurs différentes, mais de dimensions bien limitées et dont nous connaissions les vitesses de chute libre ; de cette façon nous pouvons suivre aisément le classement.

Nous pouvons décrire les phénomènes observés de la façon suivante :

1er cas. On considère un mélange de deux poudres de même densité mais de granulométries différentes (nous avons employé deux fractions de sable de quartz, classées par lévigation et dont une a été colorée en bleu).

Il n'y a classement que si la différence des diamètres moyens est suffisante. (telle que $V_1 = 2\ V_2$). Pour des différences de granulométrie plus faibles, et aux fortes concentrations il n'y a aucun classement, le lit reste homogène aussi longtemps que dure l'expérience.

Nous avons là une confirmation du processus expliqué ci-dessus : il n'y a pas de classement.

Dans le 2e cas, on considère un mélange de deux poudres de densités différentes (par exemple du sable et du charbon, ou bien du sable et du ferro silicium).

VOL. 3 1954

Il y a trois possibilités :

(a) La vitesse de chute libre du solide le plus lourd est la plus grande. On observe alors que le classement se fait rapidement, le solide le plus dense et à grande vitesse de chute occupe le bas du lit, le solide le plus léger et à plus faible vitesse de chute occupe la partie supérieure, après un délai de quelques minutes la limite entre les deux zones devient définitivement bien nette.

Ce classement a lieu même si les vitesses de chute libre sont très proches l'une de l'autre.

(b) Une deuxième possibilité est que les vitesses de chute libre soient identiques. les diagrammes $\epsilon = f(u)$ des deux poudres sont confondus.

Dans ce cas on observe qu'il y a un classement : le solide le plus dense va occuper la partie inférieure du lit. On *ne* peut *pas* expliquer ce classement par une différence entre les vitesses de chute des grains.

(c) Dans le troisième cas, où la vitesse de chute libre des grains denses est plus petite que celle des grains légers, le classement se produit encore : les grains denses à faible vitesse de chute occupent la partie inférieure du lit. Tout se passe comme si les deux poudres formaient des phases séparées et se comportaient comme des liquides non miscibles.

On peut expliquer ce phénomène par le même processus que précédemment.

Les grains de faible densité ont une plus grande vitesse de chute libre, ils sont donc beaucoup plus gros que les autres, il y a dans leur voisinage une forte réduction de la section libre offerte au liquide qui provoque une augmentation locale de la vitesse, suffisante pour les entraîner vers le haut, malgré leur plus grande vitesse de chute libre.

D'autre part, un classement en sens inverse, qui conduirait la poudre la plus légère dans le bas du lit est impossible puisqu'il donnerait lieu à une situation instable avec une phase plus légère en dessous d'une phase plus lourde.

Une dernière expérience met bien en évidence l'importance de cette question de stabilité.

On mélange deux poudres dont les vitesses de chute sont suffisemment différentes pour que

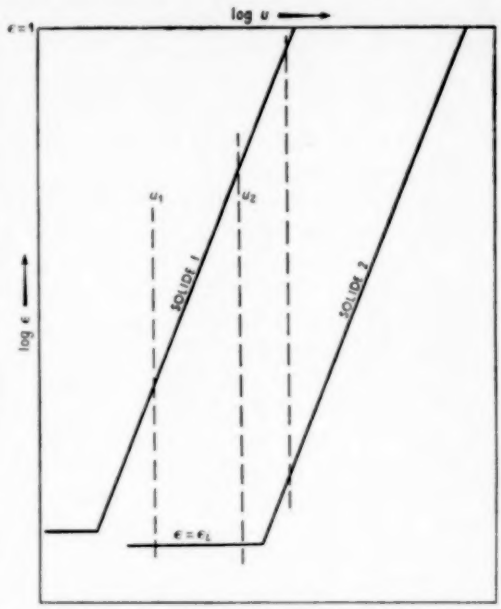

Fig. 2. Représentation de la fluidisation simultanée de deux solides.

les domaines de fluidisation ne se superposent pas : (Fig. 2).

La poudre la plus dense (1) a une plus petite vitesse de chute.

Pour une vitesse u_1, la poudre 2 n'est pas encore fluidisée, elle se sépare néanmoins de la poudre 1 qui, elle, est bien fluidisée à cette vitesse, mais chose assez remarquable elle occupe la partie supérieure du lit.

Les grains sont trop gros pour être soulevés individuellement et mis en mouvement par le liquide à cette vitesse, mais l'ensemble du lit encore compact vient flotter au-dessus du lit fluidisé formé par les grains plus denses.

On voit donc que le facteur primordial dans cette étude du classement des lits fluidisés est la densité moyenne des phases fluidisées formées par chacun des constituants du mélange pris séparément.

Si nous augmentons la vitesse du liquide, le lit de solide 1 continue à gonfler, à s'étendre, sa densité moyenne diminue, pour une vitesse u_2 cette densité devient plus faible que celle du lit 2 qui ne varie pas, on observe alors un renversement, après une période où les deux poudres sont

mélangées un nouveau classement se fait dans lequel la poudre 2 occupe la partie inférieure et la poudre 1 la partie supérieure du lit.

Le calcul montre que ce renversement se produit bien à la vitesse où la densité des deux lits devient égale.

Un mélange de deux poudres peut donc selon la vitesse du liquide se classer de deux façons diamétralement opposées, cela prouve que le classement dépend des propriétés globales des suspensions et non seulement des propriétés particulieres des grains.

En résumé nous dirons que le classement d'après les granulométries doit se faire dans une phase diluée ; dans un lit concentré le classement se fait selon les densités.

Nous pensons que cette étude du classement en dehors de son intérêt propre permet d'illustrer en quelque sorte l'intérêt qu' il y a à adopter la forme simple de la loi d'expansion $u = V\epsilon^{\sigma}$ ne serait-ce que comme un outil de travail constituant une première approximation.

Ce travail a été effectué au Service de Chimie Industrielle de l'Université Libre de Bruxelles, sous la Direction de Monsieur le Professeur DE KEYSER, avec l'aide d'une subvention du Fonds Tassel.

NOTATION

d = diamètre d'un grain.
D = distance entre deux grains.
e = expansion du lit, c'est-à-dire rapport de la hauteur H à la hauteur au repos H_i.
H = hauteur du lit fluidisé.
H_i = hauteur du lit au repos.
u = vitesse du liquide au-dessus du lit fluidisé.
V = Vitesse de chute libre des grains isolés dans l'eau.
ϵ = fraction du volume du lit fluidisé occupé par le liquide.
ϵ_i = fraction du volume occupé par le liquide dans le lit au repos.
σ = exposant de ϵ dans la relation empirique $u = V\epsilon^{\sigma}$.

VOL. 3 1954

BIBLIOGRAPHIE

[1]. CAMP, T. R. ; Proc. Amer. Soc. Civ. Eng. 1945 **71** 445.
[2]. HANCOCK, R. T. ; Mining Mag. 1942 179 oct.
[3]. JOTTRAND, R. ; J. Appl. Chem. **2** 1952 17.
[4]. LEWIS, E. W. and BOWERMAN, E. W. ; Chem. Eng. Prog. 1952 **48** 603.
[5]. LEWIS, W. K., GILLILAND, E. R. and BAUER, W. C. ; Ind. Eng. Chem. 1949 **41** 1104.
[6]. MILLER, P. H. and SAEMAN, W. C. ; Chem. Eng. Progr. 1947 **43** 667.
[7]. NEEDHAM, L. W. and HILL, N. W. ; Fuel 1947 **26** 101.
[8]. SMIRNOF, N. I. and LI DE EP ; Zhur. Priklad. Khim. 1951 **24** 383-439.
[9]. STEINOUR, H. H. ; Ind. Eng. Chem. 1944 **36** 618, 840, 901.
[10]. VERSCHOOR, H. ; Appl. Sci. Res. 1949 **A2** 155.
[11]. WILHELM, R. H. and KWAUK, M. ; Chem. Eng. Progr. 1948 **44** 201.

Chemica Engineering Science, 1954, Vol. 3, pp. 17 to 25. Pergamon Press Ltd.

A convenient method for the evaluation of vapour-liquid equilibria of binary mixtures

W. Jost and H. Röck

Institut f. Physikalische Chemie d. Universitat, Göttingen

(*Received* 1 *January* 1954)

Summary—In the evaluation of thermodynamic measurements of mixtures a development of the excess Gibbs free energy, $\Delta\overline{G^E}$, in orthogonal functions has proved advantageous. Since measurements do not give a smooth curve but a set of discontinuous values, a method appropriate for the evaluation of equidistant discontinuous measurements has been developed, using Vettin's discontinuous orthogonal polynomials. The necessary formulae and tables are listed in this paper.

Résumé—Pour l'estimation des propriétés thermodynamiques des solutions, il est intéressant de développer en séries orthogonales la fonction $\Delta\overline{G^E}$, énergie libre d'excès de Gibbs (ou enthalpie libre d'excès).

Comme les expériences ne donnent pas une courbe régulière mais une série de valeurs discontinues, il a fallu développer une méthode convenable pour l'évaluation de mesures discontinues équidistantes, en recourant aux fonctions polynomiales discontinues de Vettin. Formules et et tables nécessaires dans le mémoire.

The method generally adopted in the evaluation of equilibrium measurements of binary liquid mixtures [1] consists in a power series development of the molar excess (Gibbs) free energy $\Delta\overline{G^E}$. This series is related to the so-called Margules [2] series. Its most appropriate form, probably, is the symmetrical development, introduced by Redlich and Kister [3].

$$\Delta\overline{G^E} = B\,\xi_1\,\xi_2 \sum_0^n a_k x^k;\quad x = 2\xi_1 - 1 = \xi_1 - \xi_2. \tag{1}$$

The determination of the constants a_k becomes particularly simple if special values of ξ are preferred in the evaluation. This advantage, at the same time, implies a weakness of the method : the constants are not determined in such a way as to give, on the average, best agreement with all experimental points.

Our aim has been to find a method of representing the results which

(*a*) gives on the average optimum agreement with all experimental points, and

(*b*) furnishes a final determination of the constants entering the development.

By (*b*) the following is meant : if the coefficients of the first n members of the development have been determined, and if it is found out that this development is unsatisfactory then we try a development with $m > n$ members of the series ; the first n constants, however, need not be determined anew, but retain their original values. A development in orthogonal functions complies with our requirements, as, for instance, a Fourier series development, which, however, is not the suitable solution for our problem. Considering that the first two terms in the development (1) correspond to P_0 and P_1, the first two Legendre polynomials (spherical harmonics) [4] of $x = 2\xi_1 - 1$, varying from -1 to $+1$, the obvious development is

$$\frac{\Delta\overline{G^E}}{B\,\xi_1\,\xi_2} = f(x) = \sum_0^n A_k\,P_k(x). \tag{2}$$

Here the Legendre polynomials of the first kind are defined by

$$P_k(x) = \frac{1}{2^k\,k!}\frac{d^k}{dx^k}(x^2-1)^k, \tag{3}$$

the first 6 polynomials being

$$\begin{aligned} P_0(x) &= 1 \\ P_1(x) &= x \\ P_2(x) &= \tfrac{1}{2}(3x^2 - 1) \\ P_3(x) &= \tfrac{1}{2}(5x^3 - 3x) \\ P_4(x) &= \tfrac{1}{8}(35x^4 - 30x^2 + 3) \\ P_5(x) &= \tfrac{1}{8}(63x^5 - 70x^3 + 15x) \end{aligned} \tag{4}$$

The coefficients A_k are given by the relation

$$A_k = (k + \tfrac{1}{2})\int_{-1}^{+1} f(x)\,P_k(x)\,dx \tag{5}$$

which corresponds to the analogous equation for a Fourier development and is easily understood.

This development is satisfactory in every respect, if a continuous curve (for instance by graphical interpolation) for the experimental values is available. Especially, it allows of an unambiguous, straightforward determination of the coefficients.

If, however, the experimental points are not sufficiently closely spaced, systematic errors still may be introduced by the arbitrariness left in drawing a smooth interpolating curve. Consequently, we were looking for a procedure offering the advantages of a development in orthogonal functions, but making use only of a discrete set of measured values. At this point the advice of Professor A. WALTHER, Darmstadt, was of decisive help to us. He drew our attention to VETTIN's [5] discontinuous orthogonal polynomials, by which the problem is completely solved.

The authors are indebted to Professor VAN KREVELEN for calling their attention to the fact that analogous orthogonal polynomials are used in statistical theory (R. A. FISHER, "Statistical methods for Research Workers"; R. A. FISHER and F. YATES "Statistical Tables," Oliver & Boyd, London). The tables as given in this paper however are more convenient for the present purpose.

These polynomials $V_\nu(x/\omega)$ are a generalization of Legendre's polynomials, valid for a discrete set of equidistant measurements, defined in such a way that

$$\lim_{\omega \to 0} V_\nu(x/\omega) = P_\nu(x) \tag{6}$$

where $P(x)$ is the Legendre polynomial, ω being the length between equidistant experimental points in Fig. 1. We now attempt a development for our function $f(x)$ (equation 2)

$$f(x) = \sum_0^n a_\nu \; V_\nu(x/\omega). \tag{7}$$

The coefficients a_ν, corresponding to the coefficients A_k of the former development in Legendre polynomials, are given now by sums (instead of the former integrals)

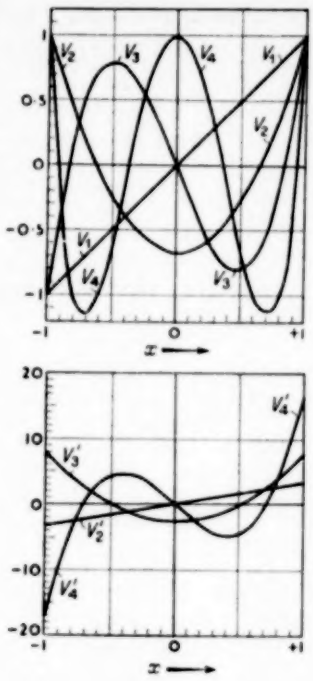

Discontinuous orthogonal polynomials $\omega = \Delta x = 0{\cdot}2$

First derivatives of the discontinuous orthogonal polynomials, $\omega = \Delta x = 0{\cdot}2$.

Fig. 1.

$$a_\nu = \frac{(2\nu+1)\,\omega}{2+\omega}\left(\prod_{\lambda=0}\frac{2-(\lambda-1)\,\omega}{2+(\lambda+1)\,\omega}\right)\times \left(\sum_{-N}^{+N} f(\eta)\; V_\nu(\eta)\right) \tag{8}$$

where $N = 1/\omega$, $\eta = x/\omega = N \cdot x$, $2N+1$ being the number of equidistant experimental points (including the two points corresponding to the two pure components). η and N are introduced only as variables for the summation. The first Vettin polynomials are

$$V_0 = 1$$

$$V_1 = x$$

$$V_2 = \frac{1}{2-\omega}\left(3x^2 - (1+\omega)\right)$$

$$V_3 = \frac{1}{(2-\omega)(2-2\omega)} + \left(10x^3 - (6+6\omega-2\omega^2)x\right)$$

$$V_4 = \frac{1}{(2-\omega)(2-2\omega)(2-3\omega)} + \left(\begin{matrix}35x^4-(30+30\omega-25\omega^2)x^2 \\ +(3+6\omega-3\omega^2-6\omega^3)\end{matrix}\right). \tag{9}$$

VOL. 3 1954

If the functions $V_\nu(x/\omega)$ and the factors $f_{a\nu}$ are tabulated (cf. the tables, App. I).

$$f_{a\nu} = \frac{(2\nu+1)\,\omega}{2+\omega} \prod_{\lambda=0}^{\nu} \frac{2-(\lambda-1)\,\omega}{2+(\lambda+1)\,\omega} \qquad (10)$$

then the evaluation of the coefficients a_ν requires a summation of products only : $\Sigma\, f(\eta)\, V_\nu(\eta)$, which is quickly done by means of any computing machine. The necessary tables are very short, because values for a discrete set of arguments only are needed.

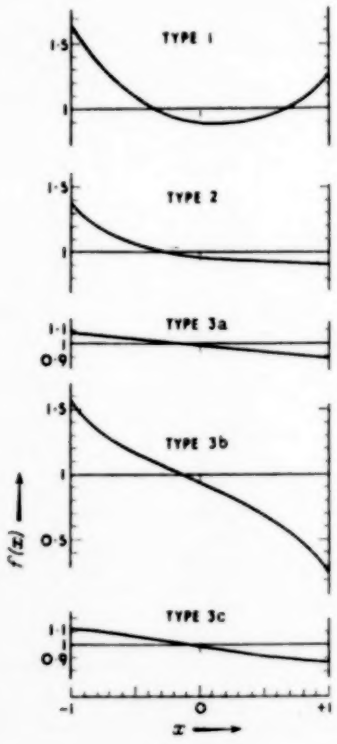

Fig. 2.

The only drawback of this method, still remaining, consists in the fact that equidistant experimental points are required. This, however, is not of a serious nature. If one carries out measurements, it is easy to have two or more points in the vicinity of, say, 10, 20 . . . . 80, 90 mol %, and to interpolate without appreciable error for the exact values 10, 20, ... 80, 90 mol %. In the examples evaluated by us, using published results, we had to employ a graphical interpolation (of $\Delta\bar{G}^E/B\,\xi_1\,\xi_2$), cf. below, p. 22. The remaining small deviations between experimental and calculated values (of usually less than 1%) are probably due to this interpolation.

The constant B in equation (1) or (2) is arbitrary. It is convenient to use $B \approx 4\,\Delta G^E_{max}$, because then the function $f(x)$ assumes values in the vicinity of unity, cf. the typical curves in Fig. 2. Of these curves 1 and 3*a* are easily approximated by means of not more than 5 Vettin polynomials (up to V_4), the approximation for 2 is somewhat less good, more difficult is that of 3*b* and *c*.

The Gibbs-Duhem equation imposes no restrictions upon the function $f(x)$. Therefore it is legitimate to replace equation (2) by

$$f(x) = \frac{\Delta G^E}{g(x)\,B\,\xi_1\,\xi_2} \qquad (11)$$

where $g(x)$ is a non-vanishing arbitrary simple function of x, chosen in such a way as to give $f(x)$ a shape which is conveniently approximated by not too many Legendre or Vettin polynomials. This procedure is quicker than the use of more polynomials for an improvement of the approximation.

The same developments may be used for the evaluation of measurements of total pressures of binary systems where measurements of partial pressures are lacking. A decomposition of the total-pressure curve into two curves for the partial pressures is usually done by an integration of the Duhem-Margules equation. It is, however, much simpler and more straightforward to use a development for ΔG^E, consistent with the Gibbs-Duhem equation, and to determine the constants in such a way as to give best agreement on the average with measured total pressures.* This method is applicable with Vettin polynomials, with Legendre polynomials or with a simple power series development for $f(x)$. Details will be published elsewhere.

* A special case of this procedure has been applied by A. Musil [6], who used the first two or three members of the Margules series.

Appendix I

(*a*) The polynomials $V_\nu(x/\omega)$ for $\omega = 0{\cdot}2$ and $V'_\nu(x/\omega) = d/dx\,(V_\nu)$

$V_0 = 1$ $\qquad V'_0 = 0$

$V_1 = x$ $\qquad V'_1 = 1$

$V_2 = \frac{5}{9}\left(3x^2 - \frac{6}{5}\right)$ $\qquad V'_2 = \frac{10}{3}x$

$V_3 = \frac{25}{72}\left(10x^3 - 7{\cdot}12\,x\right)$ $\qquad V'_3 = \frac{25}{9}\left(\frac{15}{4}x^2 - 0{\cdot}89\right)$

$V_4 = \frac{125}{504}(35x^4 - 35x^2 + 4{\cdot}032)$ $\qquad V'_4 = \frac{625}{36}(2x^3 - x)$

$V_5 = \frac{625}{3024}(126x^5 - 159{\cdot}6x^3 + 38{\cdot}4384\,x)$ $\qquad V'_5 = \frac{625}{3024}(630x^4 - 478{\cdot}8x^2 + 38{\cdot}4384)$

(*b*) the same for $\omega = 0{\cdot}1$

$V_0 = 1$

$V_1 = x$

$V_2 = \frac{10}{19}\left(3x^2 - \frac{11}{10}\right)$

$V_3 = \frac{50}{171}(10x^3 - 6{\cdot}58\,x)$

$V_4 = \frac{500}{2907}(35x^4 - 32{\cdot}75x^2 + 3{\cdot}564)$

$V_5 = \frac{625}{5814}(126x^5 - 151{\cdot}9x^3 + 35{\cdot}2024\,x)$

$V_6 = \frac{625}{8721}(462x^6 - 678{\cdot}3x^4 + 242{\cdot}609x^2 - 12{\cdot}3532)$

$V_7 = \frac{3125}{61047}(1716x^7 - 2956{\cdot}8x^5 + 1428{\cdot}43x^3 - 168{\cdot}093\,x)$

In the following the polynomials are tabulated for $0 \leqslant x \leqslant +1$, the values for $-1 \leqslant x \leqslant 0$ are obtained by considering that V_{2n} is an even, V_{2n+1} an odd function of x.

$$V_{2n}(-x) = V_{2n}(x);\quad V_{2n+1}(-x) = -V_{2n+1}(x) \quad (1)$$

Table 1. V_ν for $\omega = 0{\cdot}2$; $\nu = 1, 2, 3, 4, 5$.

x	1	2	3	4	5
0	0	−2/3	0	1	0
0·2	1/5	−3/5	−7/15	2/3	4/3
0·4	2/5	−2/5	−23/30	−1/6	4/3
0·6	3/5	−2/30	−11/15	−1	−1/3
0·8	4/5	+2/5	−1/5	−1	−2
1	1	1	1	1	1

Table 2. V'_ν for $\omega = 0{\cdot}2$; $\nu = 2, 3, 4, 5$.

x	2	3	4	5
0	0	− 89/36	0	3003/378
0·2	2/3	− 37/18	− 115/36	1057/252
0·4	4/3	− 29/36	− 85/18	− 476/63
0·6	2	23/18	− 35/12	−2723/252
0·8	8/3	151/36	35/9	− 259/126
1	10/3	143/18	625/36	9877/252
0	0	$-2{\cdot}4722\overline{2}$	0	$7{\cdot}9444\overline{4}$
0·2	$0{\cdot}6666\overline{6}$	$-2{\cdot}0555\overline{5}$	$-3{\cdot}1944\overline{4}$	$4{\cdot}1944\overline{4}$
0·4	$1{\cdot}3333\overline{3}$	$-0{\cdot}8055\overline{5}$	$-4{\cdot}7222\overline{2}$	$-7{\cdot}5555\overline{5}$
0·6	2·00000	$1{\cdot}2777\overline{7}$	$-2{\cdot}9166\overline{6}$	$-18{\cdot}8055\overline{5}$
0·8	$2{\cdot}6666\overline{6}$	$4{\cdot}1944\overline{4}$	$3{\cdot}8888\overline{8}$	$-2{\cdot}0555\overline{5}$
1	$3{\cdot}3333\overline{3}$	$7{\cdot}9444\overline{4}$	$17{\cdot}3611\overline{1}$	$39{\cdot}1944\overline{4}$

Table 3. The factors $f_{a\nu}$ for $\omega = 0{\cdot}2$.

ν	$f_{a\nu}$
0	$1/11 = 0{\cdot}0909090\overline{90}$
1	$5/22 = 0{\cdot}27727$
2	$85/286 = 0{\cdot}26224$
3	$30/143 = 0{\cdot}20979$
4	$18/143 = 0{\cdot}12588$
5	$3/62 = 0{\cdot}048387$

Table 4. V_ν for $\omega = 0{\cdot}1$; $\nu = 1, 2, 3, 4, 5, 6, 7$.

x	2	3	4	5	6	7
0	−0·57895	0	0·61300	0	−0·88545	0
0·1	−0·56316	−0·18947	0·55728	0·36223	−0·71641	−0·78885
0·2	−0·51579	−0·36140	0·39732	0·63055	−0·26563	−1·18328
0·3	−0·43684	−0·49825	0·15480	0·72730	0·30975	−0·95372
0·4	−0·32632	−0·58246	−0·13414	0·60733	0·78762	−0·16810
0·5	−0·18421	−0·59649	−0·41899	0·27425	0·94041	0·79414
0·6	−0·01053	−0·52281	−0·63003	−0·20330	0·61858	1·32077
0·7	0·19474	−0·34386	−0·70175	−0·67544	−0·14210	0·85267
0·8	0·43158	−0·04211	−0·52632	−0·89474	−0·98946	−0·62100
0·9	0·70000	0·40000	0	−0·50000	−1·10000	−1·79992
1	1	1	1	1	1	1

VOL. 3 1954

Table 5. Factors $f_{a\nu}$ for $\omega = 0{\cdot}1$; $\nu = 0, 1, 2, 3, 4, 5, 6, 7$.

ν	$f_{a\nu}$
0	0·047619
1	0·12987
2	0·17881
3	0·18775
4	0·16414
5	0·12346
6	0·081059
7	0·046765

Sometimes it is desirable to rewrite a series of Vettin polynomials as a simple power series. We give the formulae (*a*) for $n = 4$ and $\omega = 0{\cdot}2$

$$\Sigma\, a_\nu\, V_\nu = \Sigma\, A_\nu x^\nu$$

$$A_0 = a_0 - \frac{2}{3} a_2 + a_4$$

$$A_1 = a_1 - \frac{89}{36} a_3$$

$$A_2 = \frac{5}{3} a_2 - \frac{625}{76} a_4$$

$$A_3 = \frac{125}{36} a_3$$

$$A_4 = \frac{625}{72} a_4$$

(*b*) for $n = 7$, and $\omega = 0{\cdot}1$

$$A_0 = a_0 - 0{\cdot}57895\, a_2 + 0{\cdot}60944\, a_4 - 0{\cdot}88545\, a_6$$
$$A_1 = a_1 - 1{\cdot}92399\, a_3 + 3{\cdot}78426\, a_5 - 8{\cdot}60468\, a_7$$
$$A_2 = 1{\cdot}57896\, a_2 - 5{\cdot}60025\, a_4 + 17{\cdot}38682\, a_6$$
$$A_3 = 2{\cdot}924\, a_3 - 16{\cdot}32925\, a_5 + 73{\cdot}12133\, a_7$$
$$A_4 = 5{\cdot}985\, a_4 - 48{\cdot}61105\, a_6$$
$$A_5 = 13{\cdot}545\, a_5 - 151{\cdot}35859\, a_7$$
$$A_6 = 33{\cdot}10969\, a_6$$
$$A_7 = 87{\cdot}84204\, a_7$$

It is seen that a change in the even coefficients a_{2n} affects the even coefficients A_{2n} only, and vice versa.

Appendix II

Detailed evaluation of an example. The system ethyl alcohol-toluene was chosen and measurements of Wiebe and Kretschmer [7] were evaluated. The results obtained by the authors are tabulated below, cf. Fig. 3.

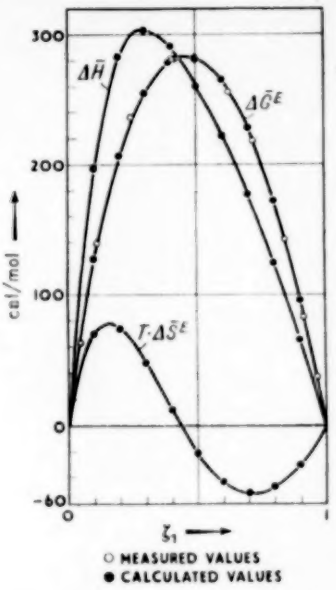

Fig. 3. Thermodynamic functions of the system ethyl alcohol – toluene at 35°C, experimental values after Kretschmer and Wiebe.

Table 1. *Experimental values for ethyl alcohol-toluene, after* Kretschmer *and* Wiebe.

ξ_1 C_2H_5OH	$\Delta\overline{G^E}$ 35°	$f(x)$ 35°	$\Delta\overline{G^E}$ 55°	$f(x)$ 55°	$T\Delta\overline{S^E}$ 35°	$\Delta\overline{H}$ 35°
0·0439	63	1·294	61	1·247	47	110
0·1157	143	1·204	137	1·150	68	211
0·2497	236	1·088	232	1·064	36	272
0·4043	280	1·003	281	1·002	− 2	278
0·4142	281	0·999	282	0·999	− 4	277
0·6282	256	0·944	258	0·948	−35	221
0·7186	219	0·933	221	0·938	−41	178
0·8423	143	0·928	147	0·949	−35	108
0·9163	83	0·933	84	0·941	−25	58
0·9635	37	0·906	38	0·927	−12	25

The function $f(x) = \dfrac{\Delta\overline{G^E}}{B\,\xi_1\,\xi_2}$ was calculated for 35°C with $B = 1160$, for 55°C with $B = 1164$. From the curve for $f(x)$ values for $\xi = 0$, 0·1, 0·2 . . . . 0·8, 0·9, 1·0 were interpolated, Table 2.

Now the coefficients a_ν of equation (8) using the notation of equation (10) must be determined. For this purpose the sums must be

computed, for instance for the determination of a_1 (with $\omega = 0{\cdot}2$)

$$a_1 = f_{a1} \cdot \Sigma f(x) \cdot V_1(x) \qquad \text{(II,1)}$$

the sum according to (8)

$$\begin{aligned}\Sigma f(x) \cdot V_1(x) = & f(-1)\, V_1(-1) \\ & + f(-0{\cdot}8)\,(-0{\cdot}8) \\ & + \cdots + f(0{\cdot}8)\, V_1(0{\cdot}8) \\ & + f(1)\, V_1(1) \qquad \text{(II,2)}\end{aligned}$$

Table 2. *Interpolated values for* $f(x)$, *from values of Table* 1.

ξ_1	$f(x)$ 35°	$f(x)$ 55°	x	η
0	1·381	1·321	−1	−5
0·1	1·218	1·168	−0·8	−4
0·2	1·117	1·087	−0·6	−3
0·3	1·044	1·038	−0·4	−2
0·4	1·002	1·002	−0·2	−2
0·5	0·971	0·975	0·0	0
0·6	0·950	0·957	0·2	1
0·7	0·936	0·949	0·4	2
0·8	0·929	0·945	0·6	3
0·9	0·919	0·940	0·8	4
1·0	0·909	0·930	1·0	5

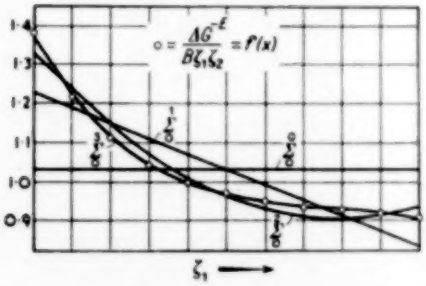

Fig. 4. Example of approximation by means of discontinuous orthogonal polynomials ; ΔG^E for ethyl alcohol-toluene at 35°C.

These sums and the corresponding coefficients a_ν for 35°C and 55°C are listed in Table 3, for $\nu = 0, 1, 2, 3, 4$.

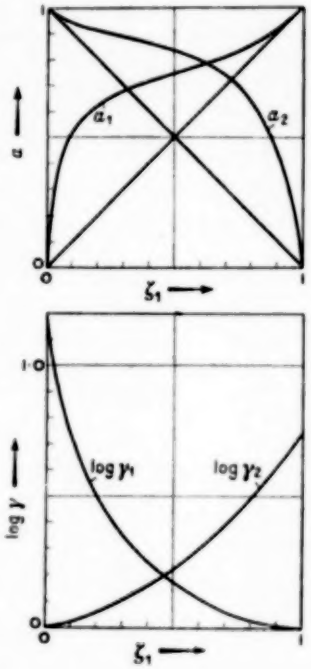

Activities of ethyl alcohol-toluene, 35°C, calculated by means of $\Delta G^E = B\,\xi_1\,\xi_2\,\Sigma a_\nu V_\nu$.

Activity coefficients of ethyl alcohol-toluene, 35°C calculated by means of $\Delta G^E = B\,\xi_1\,\xi_2\,\Sigma a_\nu V_\nu$.

Fig. 5.

In the following table the results obtained for the first, second, third and fourth approximations (up to $\nu = 1, 2, 3, 4$) are compared with experimental values $f(x)$, and for the fourth approximation the ratio $\epsilon_\nu = \dfrac{\Sigma\, a_\nu\, V_\nu}{f(x)}$ is given in the last column. $(\epsilon_\nu - 1)\,100$ is the percentage deviation, and it is seen that the maximum at 35°C is 0·35‰ at 55°C 0·83‰.

Table 3

ν	$\Sigma f(x) \cdot V_\nu$ 35°	a_ν 35°	$\Sigma f(x) \cdot V_\nu$ 55°	a_ν 55°	$\dfrac{\Delta a_\nu}{\Delta T}$
0	11·376	1·0342	11·312	1·0284	$-2{\cdot}91 \cdot 10^{-4}$
1	−0·8776	−0·1995	−0·7032	−0·1598	$1{\cdot}982 \cdot 10^{-3}$
2	0·3979	0·1043	0·3385	0·08878	$-7{\cdot}78 \cdot 10^{-4}$
3	−0·1673	−0·0351	−0·1520	−0·03189	$1{\cdot}61 \cdot 10^{-4}$
4	0·04933	0·00621	0·06081	0·00766	$0{\cdot}73 \cdot 10^{-5}$

VOL. 3 1954

The ϵ_ν's, equal to the ratio of calculated sums and $f(x)$ as obtained by interpolation between values derived from experiment, show the rapidity of convergence of the method. In order to show this more figures have been retained than are justified by the accuracy of the values $\Delta\overline{G^E}$ listed in Table 1. It should be kept in mind, however, that any function $f(x)$ or $\Delta\overline{G^E}$ may be approximated in this way. For a comparison with experiment and for a test of the thermodynamic consistency of the experiments it is necessary to calculate backwards the individual P_i (or $\Delta\mu_i^E$) or the total pressure P. In this procedure in addition to the absolute values of $f(x)$, its derivatives, too, appear. The accuracy obtained may be judged from Table 4*a*.

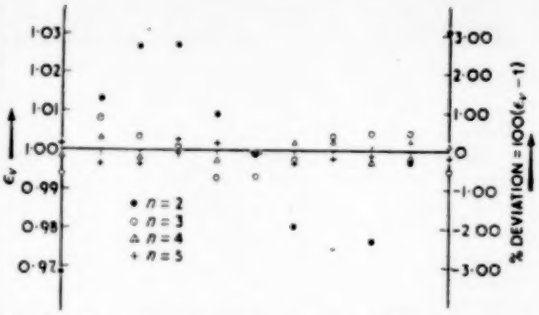

Fig. 6. Deviations from experimental values for several approximations by means of discontinuous orthogonal polynomials $\Delta\overline{G^E}$ for ethyl alcohol-toluene at 35°C.

Table 4.

x	$f(x)$	$\overset{1}{\underset{0}{\Sigma}}$	$\overset{2}{\underset{0}{\Sigma}}$	$\overset{2}{\underset{0}{\Sigma}}$	$\overset{4}{\underset{0}{\Sigma}}$	ϵ_4	
−1	1·381	1·2336	1·3378	1·3731	1·3838	0·9988	
−0·8	1·218	1·1936	1·2353	1·2285	1·2142	1·0035	
−0·6	1·117	1·1537	1·1469	1·1212	1·1136	0·9982	
−0·4	1·044	1·1140	1·0722	1·0453	1·0497	1·0003	
−0·2	1·022	1·0741	1·0115	0·9951	1·0046	0·9973	
0·0	0·971	1·0342	0·9646	0·9646	0·9709	0·9999	35°C
0·2	0·950	0·9943	0·9317	0·9481	0·9467	1·0023	
0·4	0·936	0·9544	0·9127	0·9396	0·9332	1·0027	
0·6	0·929	0·9145	0·9076	0	0·9284	0·9979	
0·8	0·919	0·8746	0·9164	0·9234	0·9252	0·9980	
1·0	0·909	0·8347	0·9391	0·9040	0·9057	1·0013	

x	$f(x)$	$\overset{1}{\underset{0}{\Sigma}}$	$\overset{2}{\underset{0}{\Sigma}}$	$\overset{3}{\underset{0}{\Sigma}}$	$\overset{4}{\underset{0}{\Sigma}}$	ϵ_4	
−1	1·321	1·1882	1·2770	1·3089	1·3165	0·9966	
−0·8	1·168	1·1562	1·1917	1·1854	1·1777	1·0083	
−0·6	1·087	1·1243	1·1183	1·0950	1·0873	1·0003	
−0·4	1·038	1·0923	1·0568	1·0323	1·0313	1·0004	
−0·2	1·002	1·0603	1·0071	0·9922	0·9973	0·9953	
0·0	0·975	1·0284	0·9692	0·9692	0·9768	1·0019	55°C
0·2	0·957	0·9964	0·9431	0·9580	0·9631	1·0064	
0·4	0·949	0·9644	0·9289	0·9534	0·9521	1·0033	
0·6	0·945	0·9325	0·9266	0	0	0·9971	
0·8	0·940	0·9005	0·9360	0·9442	0·9348	0·9944	
1·0	0·930	0·8686	0·9573	0·9254	0·9331	1·0033	

It should be considered however that deviations may partly be due to inaccuracies involved in the interpolation.

Table 4a.

ξ_1	P_{calc}	P_{obs}	$P_{obs}-P_{calc}$	$\xi_1''_{calc}$	$\xi_1''_{obs}$	$\xi_1''_{obs}-\xi_1''_{calc}$
0·0330	77·63	79·38	+1·75	0·4138	0·4216	0·0078
0·0468	84·90	86·34	+1·44	0·4687	0·4749	0·0062
0·1214	102·01	102·09	+0·08	0·5710	0·5662	−0·0048
0·2079	107·93	108·93	+1·00	0·6030	0·6014	−0·0016
0·3620	113·49	114·26	+0·77	0·6373	0·6346	−0·0027
0·4160	114·99	115·34	+0·35	0·6494	0·6384	−0·0110
5·9300	117·63	117·90	+0·27	0·6809	0·6730	−0·0079
0·7263	118·22	118·57	+0·35	0·7149	0·7164	0·0015
0·8519	116·11	116·56	+0·45	0·7836	0·7848	−0·0012
0·9701	107·34	107·64	+0·30	0·9335	0·9318	0·0017

ξ_1 = mole fraction ethanol in liquid
ξ_1'' = mole fraction ethanol in vapour
P = total pressure, Torr, at 35°C
obs = observed values
calc = calculated values with $f(x) = \sum_0^4 a_\nu V_\nu$

In addition the functions

$$T \cdot \Delta\overline{S^E} = \xi_1 \xi_2 T B \sum_0^n \sigma_\nu V_\nu ; \quad \sigma_\nu = -\frac{\partial a_\nu}{\partial T} \qquad \text{(II,3)}$$

and

$$\Delta\overline{H} = \xi_1 \xi_2 B \sum_0^n \lambda_\nu V_\nu ; \quad \lambda_\nu = a_\nu + T\sigma_\nu \qquad \text{(II,4)}$$

$$\frac{\partial}{\partial T}\left(\frac{a_\nu}{T}\right) = -\frac{\lambda_\nu}{T^2} \qquad \text{(II,5)}$$

were computed. Here B was considered as constant, which is legitimate because it changes less than 0·4% from 35 to 55°C. The last equation (II,5) allows of a calculation of the a_ν's for other temperatures, according to

$$\frac{a_\nu}{T} = \left(\frac{a_\nu}{T}\right)_{T=T_0} - \int_{T_0}^{T} \frac{\lambda_\nu}{T^2}\, dT \qquad \text{(II,6)}$$

The equations thus obtained are

$$\begin{aligned}
\Delta\overline{G^E}_{35^\circ} &= 1160 \cdot \xi_1 \cdot \xi_2 \cdot \{1{\cdot}0342 - 0{\cdot}1995 V_1 + 0{\cdot}1043 V_2 \\
&\quad - 0{\cdot}0351 V_3 + 0{\cdot}00621 V_4\} \\
\Delta\overline{G^E}_{55^\circ} &= 1164 \cdot \xi_1 \cdot \xi_2 \cdot \{1{\cdot}0284 - 0{\cdot}1598 V_1 + 0{\cdot}08878 V_2 \\
&\quad - 0{\cdot}03189 V_3 + 0{\cdot}00766 V_4\} \qquad \text{(II,7)} \\
-\Delta\overline{S^E} &= 0{\cdot}1160 \cdot \xi_1 \cdot \xi_2 \cdot \{-2{\cdot}91 + 19{\cdot}82 V_1 - 7{\cdot}78 V_2 \\
&\quad + 1{\cdot}61 V_3 + 0{\cdot}073 V_4\} \\
\Delta\overline{H} &= 1160 \cdot \xi_1 \cdot \xi_2 \cdot \{0{\cdot}9443 - 0{\cdot}4116 V_1 - 0{\cdot}1375 V_2 \\
&\quad - 0{\cdot}0145 V_3 + 0{\cdot}0039 V_4\}
\end{aligned}$$

The numerical values for 35°C are listed in Table 5.

Table 5. Thermodynamic functions for the system ethyl alcohol-toluene, at 35°C.

ξ_1	$\Delta\overline{G^E}$	$T\Delta\overline{S^E}$	$\Delta\overline{H}$
0	0	0	0
0·1	127·6	69·6	197·2
0·2	206·9	75·3	282·3
0·3	254·4	48·8	303·2
0·4	278·2	12·0	290·2
0·5	281·5	−21·0	260·5
0·6	265·1	−43·0	222·1
0·7	228·6	−51·7	176·9
0·8	172·1	−47·2	124·9
0·9	95·8	−30·4	65·4
0	0	0	0

The complete evaluation of this system, by means of a normal calculating machine, took about 4-5 hours. Included in this time is the repetition of all important steps of the calculation, for control.

Acknowledgment

The authors are indebted to Professor A. Walther, Darmstadt, Institut für Praktische Mathematik, for calling their attention to the discontinuous orthogonal functions.

Notation

$\Delta\overline{G^E}$ = molar excess Gibbs free energy, cal/mol
B = a constant of dimension, cal/mol
ξ_1, ξ_2 = mole fractions of components 1 or 2 respectively
x = symmetrical variable, $x = 2\xi_1 - 1$
a_k, a_ν = constants
P_k = Legendre polynomial of kth order
V_ν = Vettin's polynomial of νth order
$\Delta\overline{S^E}$ = molar excess entropy, cal/mol °K
$\Delta\overline{H}$ = molar heat of mixing, cal/mol
σ_ν, λ_ν = constants

Note added in proof :

A complete survey of the problem of " least squares fitting of data by means of polynomials " has been given by Birge, R. T. and Weinberg, I. W. ; Rev. Mod. Phys. 1947 **19** 298.

References

[1] Wohl, K.; Trans. Amer. Inst. Chem. Engrs. **42** 215 1946.

[2] Margules, M.; Sitzber. Akad. Wiss. Wien; Math.-nat. K.2 (II) 1898 **104** 1243.

[3] Redlich, O. and Kister, T. A.; Ind. Eng. Chem. 1948 **40** 345.

[4] Jahnke- Emde, Tafeln Nöherer Funktionen.

[5] Approximation empirischer Funktionen diskreter Verteilung durch diskontinuierliche orthogonale Polynome ZWB Ber. Nr. 2091 (1944).

[6] Musil, A. ; Z. Elektrochem 1952 **56** 995, and other publications.

[7] Kretschmer, C. B. and Wiebe, R.; J. Amer. Chem. Soc. 1949 **71** 1793.

Chemical Engineering Science, 1954, Vol. 3, pp. 26 to 35. Pergamon Press Ltd.

The distribution of residence-times in an industrial fluidised reactor

P. V. Danckwerts, J. W. Jenkins and G. Place

Department of Chemical Engineering, Tennis Court Road, Cambridge, England

(*Received* 8 *February*, 1954)

Summary—The distribution of residence-times of the gas flowing through a fluidised catalyst regenerator has been determined by using helium as a tracer. Only about 5% of the gas spends less than half, and about 5% more than twice, the mean residence-time in the regenerator. It appears that the flow through the fluidised bed itself is much closer to piston-flow than to complete mixing, the hold-back being less than 0·1.

Résumé—En utilisant l'hélium comme indicateur, les auteurs ont étudié la distribution des " durées de séjour " d'un gaz qui s'écoule au travers d'un régénérateur de catalyseur fluidisé. Tandis que 5% de la masse totale du gaz présente une " durée de séjour " inférieure à la moitié de la valeur moyenne, il y en a aussi 5% dont la " durée de séjour " dépasse le double de cette valeur. Il semble qu'au travers d'un lit fluidisé, l'écoulement gazeux se rapproche beaucoup plus d'une veine cylindrique rigide que d'un régime turbulent, la " rétension " reste inférieure à 0·1.

When gas flows through a fluidised bed of solid particles, there is a considerable spread of residence-times; different molecules of entering gas spend different lengths of time in passage, so that part of the gas spends less, and part more than the average length of time in the bed. This spread of residence-times, which is caused by back-mixing, or departure from piston-flow, is one of the most important characteristics of a fluidised reactor, as it will influence the nature and rate of the reaction. As yet, however, there is very little published information on the subject.

Gilliland and his co-workers [3] have measured the distribution of residence-times (and related characteristics) in model fluidised beds. However, there is no certainty that these reproduce the behaviour of the large-scale beds used industrially. For instance, in small beds the solid material can be seen to follow a circulatory path, with dimensions determined by those of the confining vessel, and this circulation of the solid helps to bring about back-mixing of the gas [3]. However, it is not possible to predict the way in which this motion will develop as the absolute dimensions of the bed are increased. It would be exceedingly difficult, perhaps impossible, to ensure rigorous dynamical similarity between fluidised beds whose linear dimensions are in the proportion of, say, 120 to 1 (40 ft to 4 in.). Such similarity was not attempted in Gilliland's work.

Some of the difficulties involved in the use of models can be avoided by carrying out experiments on industrial equipment. Other difficulties then arise, however; for instance, the points at which measurements are made are often dictated by their accessibility, and it is not usually possible to cover a great range of variables. Nevertheless, information obtained in this way may provide a wholesome test of the value of data obtained in the laboratory, as well as being specifically applicable to the equipment on which the experiments are made.

The only published work which provides information on the distribution of residence-times in a large fluidised bed is that of Askins *et al* [1]. Samples of gas were taken from a number of points in a cracking-catalyst regenerator. The uniformity of composition of these samples suggested that the gas in the bed was completely mixed; however, there was reason to suppose that the samples were not truly representative of the gas passing the sampling-points, since proportionately less gas was drawn from the " bubbles " which occur in the bed than from the interstitial gas flow. This phenomenon was also encountered by Gilliland and Mason [3].

The experiments described here were carried

out on a catalyst regenerator virtually identical with that used by ASKINS *et al* [2] although the air-rate and quantity of catalyst may have differed in the two cases.

A study of the residence-times of gas in a blast-furnace, using radon as a tracer, was carried out by VOICE [6], and has some points of similarity with the work described here.

GENERAL PRINCIPLES

The problem of defining and measuring the distribution of residence-times in continuous-flow systems has been discussed elsewhere by DANCKWERTS and by other authors ([2], [3], [4], [5]). In outline, the method adopted here was to inject a dose of tracer (helium) at the entrance to the system, and to determine its time-distribution in the outflowing stream.

Fig. 1 is a diagrammatic view of the regenerator. Spent catalyst from the reactor is blown up the catalyst riser by a stream of air and enters the bottom cone of the regenerator. Between the bottom cone and the main body of the regenerator is a grate-like grid. The area of the slots in the grid which allows the passage of gas and catalyst is approximately 10% of the total cross-section of the cylindrical part of the regenerator. Catalyst drawn from above the grid passes down two pipes to the catalyst recycle coolers (only one is indicated on the diagram); the catalyst is blown up through the coolers into the bottom cone by a stream of air. Roughly half the air enters the regenerator via the main riser, the remainder entering with the recycled cooled catalyst and through the pipe A. The regenerated catalyst is withdrawn from the space above the grid, and the gases pass out via the cyclones and the stack.

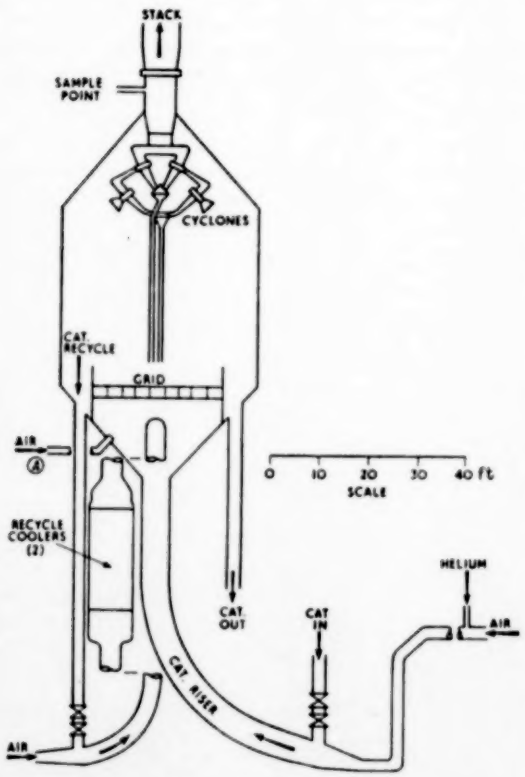

Fig. 1. Fluidised catalyst regenerator.

The procedure in these experiments was to inject rapidly a measured amount of helium into the air-line to the catalyst riser, and subsequently to take a series of samples of the stack gas at measured intervals. The ratio of helium to nitrogen was determined in these samples. Helium was used as a tracer (*a*) because of its unique molecular weight, which enables it to be estimated easily by mass-spectrometry; (b) because there is a negligible amount normally present in the stack gas; (*c*) because it would not be adsorbed by the catalyst.

The amount of information which can be derived from such an experiment depends on the validity of a cumulative series of assumptions.

(*a*) Assuming no gross experimental errors, and provided the injection is completed in a time much less than the mean residence-time in the regenerator (*c.* 30 secs) (a condition fulfilled in these experiments), the experiment gives unequivocally the distribution of residence-times of the helium atoms in their passage from the injection-point to the sampling-point.

(*b*) Assuming that molecular diffusion and gravitational convection play a negligible part in determining the paths of gas-molecules in the regenerator, in view of the high flow-velocities reigning in most regions; and that the injected helium is uniformly and rapidly spread over the cross-section of the air-pipe by turbulence

(Re $\approx 1{\cdot}5 \times 10^6$); then the distribution of residence-times of the nitrogen which enters via the riser will be the same as that of the helium. The helium can then be regarded as "labelling" the nitrogen with which it enters.

(*c*) Assuming that the spread of residence-times between the injection-point and the bottom of the regenerator is very small (i.e. all the helium atoms enter the regenerator in a time much less than the mean residence-time in the regenerator) and that the time of passage between these points (c. 5 sec) can be calculated, it is possible to find the distribution of residence-times of the nitrogen in the regenerator itself.

(*d*) Virtually all the air entering the regenerator does so by roughly the same path, as it enters via the bottom cone below the grid. The stream of air and catalyst entering via the riser is split by a distributor into a number of non-vertical streams. The interaction of these with the streams entering from the catalyst coolers and by pipe A no doubt gives rise to a high degree of agitation in the space below the grid. If it is assumed that this brings about perfect mixing in this space (i.e. entering gas molecules are rapidly and uniformly dispersed throughout the space) then the distribution of residence-times will be the same for nitrogen entering by any of the various routes. The experiment can then be taken to give the distribution of residence times of the nitrogen flow as a whole in its passage through the regenerator.

The quantity of nitrogen leaving with the regenerated catalyst is known to be negligible in comparison with the total flow, so that virtually all nitrogen leaves through the stack. A small amount of fluidising air is put into the downcomers to the recycle coolers, and it is considered that this prevented any significant amount of helium being carried round the recycle cooling circuits; the residence-times measured therefore refer to the regenerator exclusive of the coolers.

EXPERIMENTAL

Helium Injection—The helium was introduced from the storage cylinder into a pressure-vessel from which air had been displaced by filling it with water. The volume of gas in the vessel was about 1·3 cu. ft. and the pressure about 150 p.s.i.g. before and about 50 p.s.i.g. after helium had been released into the air-line. The pressure-vessel was connected to the air-line by a $\frac{3}{4}$ in. pipe about 3 ft. long, which was closed by a simple cock. The injection of helium was accomplished by opening and closing the cock as quickly as possible. The timing drum (see below) indicated that helium was flowing into the air-line for a period of less than 0·2 sec. in both runs. The quantity of helium injected could be calculated from the ambient temperature, the volume of the pressure-vessel, the initial pressure, and the pressure after the residual gas had returned to ambient temperature. The gauge was tested after the experiment and found to be accurate.

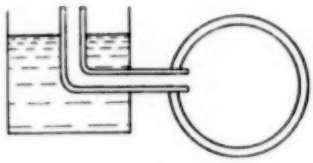

Fig. 2. Sampling pipe and branch, with cooling bath.

Sampling—Samples of the stack-gas were taken through a 4 ft. long 1 in. pipe projecting into the stack. This pipe was vented freely to the atmosphere, and the pressure-drop (9 p.s.i.) was sufficient to cause the gas to flow through the pipe at a high velocity. 12 side-branches of $\frac{1}{8}$ in. I.D. tube were brazed into the pipe, and passed through a water-bath so that their outer ends remained cool (Fig. 2). The sample vessels were attached to these branch tubes by rubber pressure-tubing. A sample vessel is shown in Fig. 3. A three-way tap C gave access either to the purge vessel or to the sample-vessel proper. Each vessel was connected via a header-pipe to a vacuum pump, and before sampling both vessels were evacuated

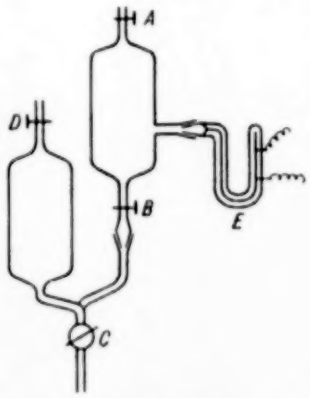

Fig. 3. Purge and sample vessels.

down to tap C, which was turned so as to isolate them from the stack-gas and from one another. Tap A was then closed (tap D could be left open if the vacuum pump

VOL. 3 1954

Run 1.

Nitrogen flow rate : $n = 1{\cdot}85$ *lb. mole/sec.*
Calculated time of passage from injection-point to base of regenerator = 5·4 *sec.*

Time after entry of He	t *(sec.)*	9·6	15·1	20·6	25·2	30·7	41·8	46·8	51·8
$(He/N_2) \times 10^6$	$10^6\, c'$	0	146	351	276	208	116	72·5	55·8
$(He/CO_2) \times 10^6$	$10^6\, a'$	0	926	2180	1850	1310	732	476	374
CO_2/N_2	c'/a'	—	0·158	0·161	0·149	0·159	0·155	0·151	0·149
$(He/N_2) \times 10^6$	$10^6.\ a'.\ (c'/a')_m$	0	143	338	286	202	116	73·5	57·7

$$\left(\frac{c'}{a'}\right)_m = 0{\cdot}155\ ; \qquad \frac{CO_2}{N_2}\ (\text{Orsat}) = 0{\cdot}148$$

Helium injected : $Q' = 0{\cdot}0195$ lb. mole ; $n\int_0^\infty c'\,dt = 0{\cdot}0149$ lb. mole

Mean residence time : $\dfrac{N}{n} = 33{\cdot}7$ sec ; $\displaystyle\int_0^\infty c'tdt \Big/ \int_0^\infty c'dt = 32{\cdot}0$ sec.

Run 2.

Nitrogen flow-rate : $n = 1{\cdot}87$ *lb. mole/sec.*
Calculated time of passage from injection-point to base of regenerator = 5·3 *sec.*

Time after entry of He	t *(sec.)*	4·7	11·0	14·2	16·2	18·6	21·2	23·1	31·7	49·7	60·1
$(He/N_2) \times 10^6$	$10^6\, c'$	0	16·6	67·0	147	198	244	256	165	46·5	23·1
$(He/CO_2) \times 10^6$	$10^6\, a'$	0	112	435	961	4350	1670	1730	1040	323	156
CO_2/N_2	c'/a'	–	0·148	0·154	0·152	0·146	0·146	0·148	0·145	0·146	0·146
$(He/N_2) \times 10^6$	$10^6.\ a'.\ (c'/a')_m$	0	16·6	64·5	143	200	248	256	154	47·9	23·1

$$\left(\frac{c'}{a'}\right)_m = 0{\cdot}148\ ; \qquad \frac{CO_2}{N_2}\ (\text{Orsat}) = 0{\cdot}148$$

Helium injected : $Q' = 0{\cdot}0191$ lb. mole ; $n\int_0^\infty c'dt = 0{\cdot}0114$ lb. mole.

Mean residence time : $\dfrac{N}{n} = 33{\cdot}5$ sec. ; $\displaystyle\int_0^\infty c'\,tdt \Big/ \int_0^\infty c'dt = 33{\cdot}3$ sec.

was kept running). When it was desired to take a sample, a rapid turn of tap C through some 220° brought about the following sequence of events : (a) the purge vessel was opened to the branch-tube, and sucked through it several times its own volume of stack-gas ; (b) the purge vessel was isolated ; (c) the sampling vessel was opened to the branch-tube and sucked in a sample of stack-gas ; (d) the sampling vessel was isolated. Tap B was closed at leisure, and the sample removed for analysis.

By this method the branch-tube was flushed out with

the gas to be sampled immediately before the sample was taken.

Time Measurements—The time of injection and the times at which the samples were taken were recorded by an electrically-operated stylus on a rotating drum. The stylus drew a horizontal line except when any one of 13 electrical circuits was closed, when it moved upwards and drew a line at a higher level so long as the circuit remained closed. The injection of helium caused one circuit to close and remain closed so long as the helium flow continued (see Fig. 4). The stylus thus recorded the time and duration of the injection. As each sample-vessel was filled, a thread of mercury rose into the evacuated arm of a small capillary-tube manometer (E, Fig. 3). In doing so it momentarily made a contact between two platinum wires, and the stylus recorded a " blip " on the drum. Action at the injection, sampling and timing-points was coordinated by field-telephone.

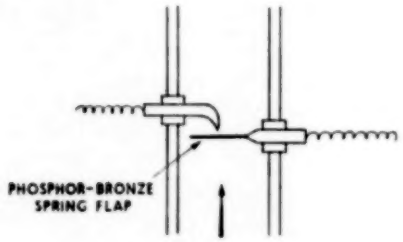

Fig. 4. Helium injection timing device.

Analyses—The samples were analysed with a Metropolitan Vickers MS2 Mass Spectrometer. No modifications were made to the instrument, which was currently in use for routine hydrocarbon gas analysis. However, in order to achieve a high sensitivity for the detection of helium (0·0005 %) the sample pressure on the high pressure side of the introduction leak to the ionization chamber was increased to 20 mm.Hg.

Some of the samples were contaminated by air which leaked into the sample vessels ; a correction was made for this by determining the ratio of O_2 to N_2 in the samples (the stack gas itself contained not more than 0·2 mol % O_2, dry basis).

The accuracy of the reported ratios of helium to nitrogen was estimated as :

$$\frac{\text{true } (He/N_2)}{\text{reported } (He/N_2)} = \frac{c}{c'} = \alpha(1 \pm \delta)$$

the error δ having a maximum value of 0·1 and the coefficient α (which was used only in the helium material balance) being a constant for the samples in any one run. The ratios of the true and reported He/CO_2 ratios were similarly related, α having the same value. It was found that at the abnormally high sample pressures, mass discriminatory effects made the absolute value of α difficult to determine. These discriminatory effects, which were absent for heavier molecules ($M > 20$) at 20 mm.Hg., and for helium atoms at lower sample pressures were thought to be due either to the onset of hydrodynamic flow, or more probably to space-charge effects within the ionisation chamber. On the basis of synthetic blends which were made up and analysed, α was at first believed to lie between 0·9 and 1·1. However, in view of the discrepancy in the helium balance (see " Interpretation of Results ") further calibrating measurements were made under conditions simulating more closely those prevailing during the analysis of the experimental samples. The calibrations indicated that α had the value of 1·33 for Run 1, and 1·49 for Run 2. The former gives a helium balance to about 1 %, but the discrepancy in the latter is still about 10 %.

INTERPRETATION OF RESULTS

The tables show the reported ratios of He to N_2(c') and He to CO_2(a'). The ratio (c'/a') should be equal to the ratio of CO_2 to N_2 in the sample, and hence should be virtually constant in each run and equal to the mean ratio obtained from the analyses of the stack-gas carried out before and after each run. This provides a useful check on the consistency of the analyses.

Multiplying the He/CO_2 ratios, a', by the mean value $(c'/a')_m$ for the run gives a second series of values of the He/N_2 ratios in each run. Since these contain independent information, they have been given equal weight with the directly-determined values of c' in plotting the distribution-curves.

From a knowledge of the dimensions of the air-pipe and catalyst-riser, and the volume of the catalyst present in the latter, it was possible to calculate the delay between the injection of the helium and its arrival at the bottom of the regenerator. This delay was subtracted from the time at which a sample was taken, to obtain the value of t, the time between the entry of the helium at the bottom of the regenerator and taking the sample. The calculation of the delay (*c.* 5 sec) was subject to the uncertainties discussed below in connection with the calculation of the mean residence-time in the regenerator, but the error involved is not thought to have been great enough to have any substantial effect on the subsequent interpretation of the results.

If c is the mole ratio of He to N_2 in the stack-gas

at time t, and n is the total rate of feed of nitrogen (which virtually all leaves by the stack), the rate of escape of He up the stack at time t is nc. Thus the total quantity Q of helium injected is given by

$$Q = n \int_0^\infty c\,dt. \qquad (2)$$

A fraction $\frac{nc}{Q} \cdot dt$ of the helium escapes between t and $(t + dt)$ – i.e. this fraction of the helium has residence-times between t and $(t + dt)$. Thus the mean residence-time of the helium as a whole is

$$\theta = \frac{n}{Q} \int_0^\infty ct\,dt$$

$$= \int_0^\infty ct\,dt \Big/ \int_0^\infty c\,dt\,. \qquad (3)$$

In order to determine Q and θ from equations (2) and (3), c' and $c't$ can be plotted against t, and the curves integrated graphically. However, each curve has a "tail" extending beyond the time of the last observation. In order to estimate the area under the tail, $\ln c'$ was plotted against t for each run, and it was found that the later values of c' in each case fell on a straight line with slope

$$-\frac{d \ln c'}{dt} = 0{\cdot}065 \text{ sec}^{-1}.$$

Assuming that the tails of the c' vs. t curves continue to obey this relationship, the relevant integrals can be easily computed. (In fact, since some helium will find its way into the pores of the catalyst, from which it will diffuse out slowly, the tail probably becomes flatter than the above expression suggests. The above method thus probably under-estimates the mean residence-time. However the discrepancy is probably not large, as the mean residence-time θ computed from equation (3) agrees well with that estimated from plant operating data. The good helium balance obtained in Run 1 also tends to support this view.)

θ can also be found by dividing the quantity N of nitrogen present in the regenerator at any instant by the nitrogen feed-rate, n :

$$\theta = \frac{N}{n}. \qquad (4)$$

N is computed from the void-volume of the regenerator and the temperature, pressure and composition of the gas. The computation is subject to various uncertainties :

(*a*) The quantity, and hence the volume, of the catalyst in the regenerator cannot be measured directly and must be inferred from the pressure drop in the catalyst bed. (The pore-volume of the catalyst was included in the total void-volume, of which it comprised about 5%.)

(*b*) The pressure fell from about 16 p.s.i.g. at the bottom to about 9 p.s.i.g. at the top of the regenerator. There was a drop of about 1 p.s.i. across the grid. Estimated average values were used for the spaces above and below the grid.

(*c*) The temperature above the grid was fairly uniform (600°C); however, there was a considerable rise in temperature between the bottom of the regenerator and the grid (from about 540 to 600°C) and an estimated average was used for this relatively small volume (5% of total void space).

(*d*) No information was available concerning the variation of composition of the gas with the level in the regenerator (although the work of ASKINS *et al* [1] suggests that it may be uniform above the grid). A uniform value of 71 mole % N_2 (wet basis) throughout the regenerator was used in the computation. This corresponds to the composition of the stack gas. Since the actual concentration of nitrogen could at no point have been greater than 79 % or less than 65%, the error introduced by this approximation was probably considerably less than 10%.

In the table of results the value of the mean residence-time has been calculated from N/n for each run, and can be compared with the value obtained by integration according to equation (3). The agreement is satisfactory considering the uncertainties involved. The values of θ obtained from equation (3) are used in subsequent calculations.

On the other hand, there is a considerable

discrepancy in each run between Q', the quantity of helium calculated from the pressure and volume of the container, and the quantity Q calculated from equation (2) and the reported helium ratios. In view of the internal consistency of each run, the agreement between the residence-times calculated by each method, and the agreement (demonstrated later) between the reduced distribution-curves for the two runs, it seems clear either that the reported quantity, Q', of helium injected was larger by a factor α (different in each run) than the true quantity Q; or that the reported helium ratios, c' and a', were smaller by a factor $\frac{1}{\alpha}$ (different but *constant* in each run) than the true ratios c and a. For the purpose of interpreting the results it makes no difference which error has occurred. In either case, $cQ'/c'Q = \alpha$, and equation (2) takes the form

$$Q' = \alpha n \int_0^\infty c' \, dt, \tag{5}$$

while equation (3) remains valid (putting c' for c). α is then found to have the values 1·31 for Run 1, 1·67 for Run 2. As explained under "Analyses," further experiments with the mass spectrometer indicated that in fact the reported values c' should be multiplied by a factor of 1·33 in Run 1, and 1·49 in Run 2. The helium balance is thus very good for Run 1; the discrepancy in Run 2 remains unexplained.

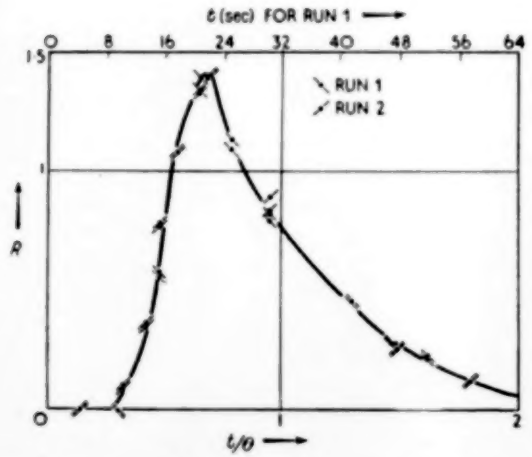

Fig. 5. *C*-diagram for Runs 1 and 2. The area under the curve between any two ordinates represents the fraction of material having residence-times between the corresponding values of t.

It is desirable to plot the results in dimensionless form, as a reduced distribution-curve, or *C*-diagram [2]. This leads to a curve which is independent of the quantity of tracer used, and which directly represents the distribution of residence-times. The ordinate, $R\{t\}$, is the ratio of the concentration of helium in a sample taken at time t to that which would be obtained by dispersing the helium uniformly throughout the regenerator, and was calculated as follows:

$$R\{t\} = \frac{Nc}{Q} = \frac{N\alpha c'}{Q'} = \frac{N\alpha c'}{\alpha n \int_0^\infty c' \, dt}$$

$$= c' \frac{\theta}{\int_0^\infty c' \, dt} = c' \frac{\int_0^\infty c' t dt}{\left[\int_0^\infty c' dt\right]^2} \tag{6}$$

The abscissa is the ratio of t to the mean residence-time:

$$t/\theta = t \frac{\int_0^\infty c' \, dt}{\int_0^\infty c' t dt}. \tag{7}$$

It will be noticed that no figures derived from the plant operating data (e.g., n, N) are involved in calculating R and t/θ by this method. Only the reported values of the He/N_2 (and He/CO_2) ratios and the measurements of time are used. Equations (6) and (7) are exact as long as the error α is constant in each run.

R is plotted against t/θ in Fig. 5 to give the *C*-diagram for each run. Since operating conditions were almost identical during the two runs, the two curves should also be identical In fact the points appear to lie on a single curve.

This is strong evidence for the internal consistency of the analyses for each run; it also suggests that the methods of evaluating $\int_0^\infty c'\,dt$ and $\int_0^\infty c't\,dt$ are not subject to any substantial errors. The area under the curve between any two values of t/θ is equal to the fraction of the material which has residence-times between the corresponding values of t.

The fraction, $F\{t\}$, of the helium (or nitrogen) spending less than a specified time, t, in the regenerator, is given by

$$F\{t\} = \int_0^t R\{t\}\,\mathrm{d}\,(t/\theta)\,. \qquad (8)$$

Values of F can therefore be obtained by graphical integration of the C-diagram, and are plotted against t/θ in Fig. 6, which is known as an F-diagram (2).

Discussion

The most striking feature of the diagrams (Figs. 5 and 6) is that none of the gas spends less than one quarter of the mean residence-time in the regenerator, and only some 5% of it spends less than half. This proves that under the conditions of

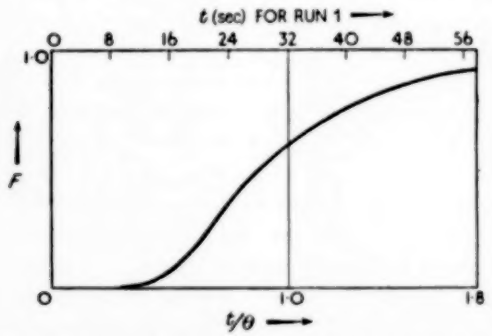

Fig. 6. F-diagram for Runs 1 and 2. The value of F for a given value of t is equal to the fraction of material spending times less than t in its passage through the system.

operation the gas in the regenerator (above the grid) is not completely mixed; in other words, there is no effective back-mixing between the top and bottom of the regenerator. The hold-back of the system is 0·17, whereas for a completely-mixed system it would be 0·37, and for piston-flow zero. (The hold-back is a measure of the departure from piston-flow, and is equal to the area under the F-diagram up to the ordinate $t/\theta = 1$; if the total quantity N of nitrogen present in the regenerator at a given instant were labelled, the hold-back would be the fraction of labelled nitrogen still present after a quantity N of unlabelled nitrogen had flowed in [2]). Only about 5% of the gas spends more than twice the mean residence-time in the system.

It is not possible to deduce from the experimental results the exact distribution of residence-times of the gas in its passage through the fluidized bed itself, since little is known *a priori* about the nature of the flow in the space above the bed, which has a profound influence on the overall distribution as measured. However, a surprising amount of information can be extracted by the method of analysis to be described.

It seems probable that the gas in the space below the grid is completely mixed, owing to the impingement of various streams at relatively high velocities. If this is so, the entering helium is instantaneously dispersed throughout the interstitial gas-space below the grid; its mean residence-time in this space is calculated (in Run 1) to have been 2·4 sec. The pressure-drop of 1 p.s.i. across the grid makes it probable that the gas flow-rate is uniform through all parts of the grid. The high velocity between the bars makes it highly unlikely that there is any back-mixing across the grid.

The height of the catalyst bed above the grid was estimated, from the pressure gradient and total pressure-drop in the bed, to be about 17 ft. (This implies a void-fraction of 0·73, excluding pores). Hence the total void-volume in the bed (including pores) was calculated to be 29% of the gas space above the grid, and the mean residence-time of the gas in the bed was taken to be 29% of that between grid and stack, or 8·5 sec.

If it is further assumed that there is no back-mixing between gas which has left the catalyst-bed and that within it, the flow through the regenerator may be represented as the flow

through three compartments which discharge into one another in series (Fig. 7).

GILLILAND and MASON [3] showed that the residence-time distribution in their model fluidised beds could be represented approximately by expressions of the form :

$$\left.\begin{aligned} F &= 0, && \frac{t}{\theta} < \frac{S-1}{S} \\ F &= 1 - e^{\left(S-1-\frac{St}{\theta}\right)}, && \frac{t}{\theta} \geqslant \frac{S-1}{S} \end{aligned}\right\} \qquad (9)$$

where S is a parameter which depends mainly on the geometry of the bed, and θ the mean residence-time in the bed. When $S = \infty$ the above expression reduces to the F-diagram for piston-flow, and when $S = 1$ we have the expression for " complete mixing." Intermediate values of S represent systems with different degrees of hold-back between these limits; the hold-back in the system is $1/Se$. Some F-diagrams with different values of S are shown in Fig. 8.

If it is assumed that the distribution in the large fluidised bed in the catalyst regenerator also conformed to equation (9), it can be shown that the value of S must lie between certain limits. Regarding the regenerator as equivalent to three compartments in series (Fig. 7) with " complete mixing " in the first (A) and a distribution corresponding to equation (9) in the second (B), it is possible to relate the observed overall distribution to the unknown distribution in the third compartment (C) by the following expression :

$$F_3\{t\} = F\{\tau\} + \left[\frac{\theta_1}{\theta} + \frac{\theta_2}{S\theta}\right] R\{\tau\} + \frac{\theta_1\,\theta_2}{S\theta^2}\left[\frac{\mathrm{d}R\{t'\}}{\mathrm{d}(t'/\theta)}\right]_{t'=\tau}, \qquad (10)$$

where $\tau = t + \theta_2\left(\frac{S-1}{S}\right)$.

In this expression $F_3\{t\}$ is the fraction of material which spends times less than t in its passage through the third compartment; θ_1, θ_2, θ are the mean residence times in A, B and the whole system respectively; and the number S, which determines the distribution in compartment B, is unknown. $F\{\tau\}$ and $R\{\tau\}$ are the values of F and R for the system as a whole (taken from Figs. 5 and 6 respectively in the present case) at a time $\tau = t + (S-1)\,\theta_2/S$; the last term (in square brackets) is the slope of the C-diagram (Fig. 5) for the whole system at time τ.

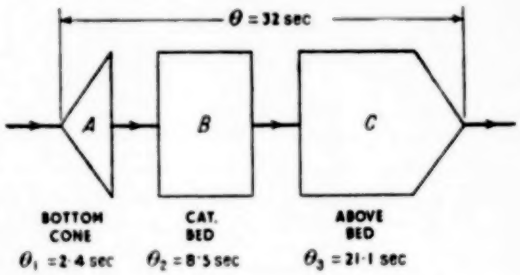

Fig. 7.

Thus, if a value is assigned to S, the corresponding F_3-diagram for the third compartment can be constructed from the data for the system as a whole. It is found by trial that if S is taken to be less than 2, the F_3-diagram has a region of negative slope, which represents a physical impossibility. If S is 5 or less the F_3-diagram displays a point of inflection (i.e. slope has a minimum value). This corresponds to a C_3-diagram with two peaks, and while such behaviour is possible for systems in which, for instance, the gas flows through two parallel and dissimilar channels, it can be confidently assumed that it does not occur in the space above the bed. The conclusion is that S must be greater than 5 for flow through the fluidised bed, the hold-back being less than 0·075. In other words (see Fig. 8) the flow of gas through the bed does not depart very far from piston-flow.

It should be emphasised that this conclusion, in its qualitative form, does not depend on the exact validity of the assumptions made, or on exact conformity with equation (9); these merely serve to simplify the calculations. Provided there is no substantial degree of back-mixing between the three " compartments," and the estimate of the void-volume of the bed is approximately correct, the experiment can be taken to show that the flow through the bed is much closer to piston-flow than to complete mixing.

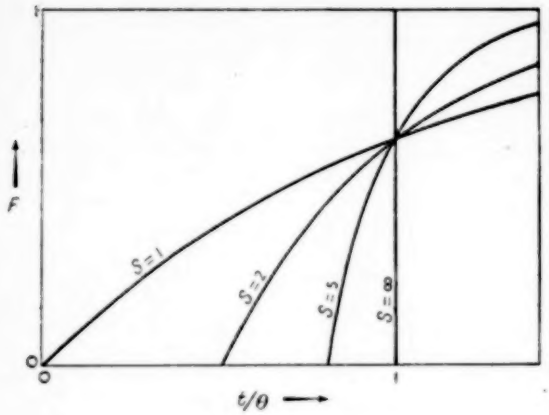

Fig. 8. $F = 1 - e^{\left(S-1-\frac{St}{\theta}\right)}$.

Conclusions

Although the distribution of residence-times for the gas flowing through the fluidised bed cannot be deduced exactly from the experiments, it can be concluded with some confidence that it is much closer to piston-flow than to complete mixing, and has a hold-back of less than 0·1.

Acknowledgment

The experimental work described was carried out during a summer vacation course at the Stanlow Refinery of the Shell Refining and Marketing Company. We are indebted to the Company for their generosity in enabling the work to be carried out and allowing the results to be published, and to the technological staff for their collaboration at all stages.

Notation

c = true mole ratio of He to N_2 in sample
c' = reported value of above
a = true ratio of He to CO_2 in sample
a' = reported value of above
Q = true quantity of He injected (lb. mole)
Q' = apparent value of above calculated from pressure change in container
$\alpha = cQ'/c'Q$
N = nitrogen contained in regenerator (lb. mole)
n = feed-rate of nitrogen to regenerator (lb. mole/sec.)
θ = mean residence time of nitrogen in regenerator (sec.)
t = time after injection of helium, less calculated time of passage from injection-point to bottom of regenerator (sec.)
$R = Nc/Q$ (see equation (4))
F = fraction of material spending less than specified time in passage
$\tau = t - \theta_2\left(\frac{S-1}{S}\right)$
S = parameter in equation (9)

Subscripts :
1, 2, 3 refer to gas-spaces below grid, in catalyst bed and above catalyst bed respectively.

References

[1] Askins, J. W., Hinds, G. P. and Kunreuther, F.; *Chem. Eng. Prog.* 1951 **47** 401.
[2] Danckwerts, P. V.; *Chem. Eng. Sci.* 1953 **2** 1.
[3] Gilliland, E. R. and Mason, E. A.; *Ind. Eng. Chem.* 1949 **41** 1191, 1952 **44** 218.
[4] Kramers, H. and Alberda, G.; *Chem. Eng. Sci.* 1953 **2** 173.
[5] Schoenemann, K.; *Dechema-Monographien* 1952 **21** 203.
[6] Voice, E. W.; *J. Iron and Steel Inst.* 1949 **163** 312, 1950 **166** 315.

Book review

W. G. Berl: Physical Methods in Chemical Analysis, Academic Press, Inc. 640 pages. Price $13.50, 1951.

As in Volume 1, each chapter in this book has been written by an expert in the field, and is concerned with a particular aspect of the use of physical methods in chemical analysis. The first chapter deals with polarography, and gives concise accounts of the theory, apparatus, and techniques used. Useful tables of depolarisation potentials are included, and over forty typical analyses are summarised. The chapter ends with a discussion of polarometric titrations. The basic features of polarography are adequately covered, and it is therefore unfortunate that only a few references to the available literature have been included for those who wish to follow the subject further. This is a general criticism of many chapters of the book. The next chapter covers the theory and technique of conductivity and conductometric titration. As a minor criticism one may note that the use of ion-exchange resins is not mentioned in the section on the preparation of conductivity water. The conductometric titration section includes phenols and alkaloids as well as inorganic acids and bases and titrations which involve precipitations are also reviewed. Potentiometric analysis is discussed in an admirable manner in the following chapter, and adequate references to literature data and reference books are given.

An excellent account of electrography and electrospot testing includes a historical survey, full details, with good diagrams, of the equipment, materials, electrolytes, reagents, etc. used, and a good review of uses in identification of pure metal surfaces, alloys, and anions. Special applications, such as the structure of steel and nonferrous metals, and a section on quantitative applications, complete this useful chapter. Adequate accounts of magnetic methods of analysis, and of the determination of the area of surfaces of solids, are followed by a chapter on surface tension measurements. This reviews competently the capillary rise, maximum bubble pressure, drop-weight and pendant drop, and ring methods of determination of surface tension, but would have been much improved by a detailed section on applications.

Vacuum techniques of analysis depend first on the production and measurement of low pressures, and a good, but perhaps over-long, account of this is given. The vacuum fusion method for the analysis of gaseous elements in metals, and the determination of carbon by low-pressure combustion are next considered in detail. The section on the micro-analysis of gases at low pressures covers only a small part of the field, however, although literature references are given to other work. A discussion of molecular distillation and a full collection of references completes this somewhat unbalanced chapter. A good account of analysis by thermal conductivity comes next, and is followed by a useful chapter on the measurement of radioactivity for tracer applications. This surveys, with the aid of excellent diagrams, the photographic and electrical methods of detection, the principles of counting, and analytical procedures. An equally useful chapter is that on statistical analysis, with particular reference to spectrography and spectrographic analysis; numerical examples are given. The final chapters surveys briefly chromatographic analysis, and is useful as an introduction to the subject.

The book is well printed, is relatively free from major errors, and on the whole provides a valuable compendium of methods and techniques of physical methods of analysis which should be available in every library.

R. N. Haszeldine